ARGONNE NATIONAL LABORATORY
9700 South Cass Avenue, Argonne, Illinois 60439

November 13, 1987

Dr. Lester S. Rubenstein
Division of Licensing
U.S. Nuclear Regulatory Commission
Washington, D.C. 20555

Dear Dr. Rubenstein:

I thought that I had sent you copies of the final manuscripts of ANL/RERTR/TM-10 and ANL/RERTR/TM-11, but when I gave them a final reading prior to sending them to be printed I found that there were still corrections to be made. None of the changes are significant--most of them involved hyphens--although a few numbers were slightly changed.

The manuscripts are now going to the printer. I am enclosing copies of the changed pages to replace the ones I sent last week.

I apologize for any inconvenience that this may cause.

Sincerely,

James L. Snelgrove

James L. Snelgrove
Coordinator, Engineering Applications
RERTR Program

Enclosures (2)

cc: R. E. Carter (INEL)
C. H. Cooper (INEL)
R. R. Hobbins (INEL)
J. E. Matos (w/o encl.)
A. Travelli (w/o encl.)

D/3

Changed Pages of ANL/RERTR/TM-11

Table of Contents

Table of Contents (Cont.)

List of Tables

The Use of U_3Si_2 Dispersed in Aluminum in Plate-Type Fuel Elements for Research and Test Reactors

1. INTRODUCTION

The U.S. Reduced Enrichment Research and Test Reactor (RERTR) Program was established by the U.S. Department of Energy in 1978 to provide the technical means to convert research and test reactors from the use of highly enriched uranium (HEU) fuel to the use of low-enriched uranium (LEU) fuel. In order to maintain the required excess reactivity of the reactor core, the amount of ^{235}U must be increased by 10 to 15% to overcome the additional neutron absorption of the greatly increased ^{238}U content in LEU fuel and the effects of a harder neutron spectrum. This additional ^{235}U and ^{238}U can be accommodated by increasing the uranium density of the fuel and/or by redesigning the fuel element to increase the volume fraction of fuel in the reactor core. The RERTR Program has vigorously pursued both paths with major efforts in fuel development and demonstration and in reactor analysis and design.[1]

Research and test reactor fuel elements consist of assemblies of fuel-containing plates or rods. The RERTR Program has concentrated its efforts on plate-type fuels since plate-type research and test reactors consume much more HEU than do rod-type reactors. High-density LEU rod-type fuels have been developed by GA Technologies for TRIGA reactors[2] and by Atomic Energy of Canada, Ltd.[3] Rod-type fuels will not be discussed further in this report.

The fuel plates used in the fuel elements for most research and test reactors consist of a fuel core, or "meat," in an aluminum alloy cladding. Originally, cast and wrought alloys of uranium and aluminum, consisting of UAl_3 and UAl_4 precipitates in an aluminum matrix, were used for the fuel meat. Fabrication of alloy cores with uranium densities above ~1.1 Mg U/m^3 is difficult, however, and powder metallurgical cores, with UAl_x (a combination of UAl_2, UAl_3, UAl_4, and Al phases) or U_3O_8 dispersed in aluminum, are now used in most cases. In 1978 the densest UAl_x fuel in use contained ~1.7 Mg U/m^3 in the fuel meat (~37 vol% UAl_x), and the densest U_3O_8 fuel in use contained ~1.3 Mg U/m^3 in the fuel meat (~18 vol% U_3O_8). The RERTR Program has developed and tested UAl_x and U_3O_8 dispersion fuels for LEU applications up to their practical fabrication limits--2.4 and 3.2 Mg U/m^3, respectively.

In order to minimize the need to redesign fuel elements to increase the fuel volume fraction and to make significant enrichment reductions in high-performance reactors even feasible, higher densities yet were needed. One approach, followed by the French Commissariat à l'Energie Atomique (CEA), utilized small wafers of sintered UO_2 contained in compartments of a fuel

plate produced by diffusion bonding Zircaloy frames, spacer wires, and cladding plates.[4] The 7%-enriched "caramel" fuel has performed well in OSIRIS;[5] however, fabricators of conventional plate-type fuels would have to implement a completely new fabrication process to produce caramel fuel.

The RERTR Program chose to pursue the use of high-density uranium-silicon alloys in place of UAl_x and U_3O_8 in conventional aluminum-matrix dispersion fuel in order to take advantage of the large commercial base of equipment for and experience in fabrication of such fuels. One uranium silicide compound, U_3Si_2, has been found to perform extremely well under irradiation and can provide a uranium density of at least 4.8 Mg/m^3.

The development and testing of uranium silicide fuels has been an international effort, involving other national reduced enrichment programs, several commercial fuel fabricators, and several test reactor operators. In particular, the testing of full-sized fuel elements has been performed cooperatively, with the U.S. Government providing the enriched uranium, the fuel fabricators providing the fabrication, and the U.S. Government or other governments providing the irradiations and postirradiation examinations.

Numerous results of the development and testing of uranium silicide-aluminum dispersion fuels have been published previously. The results for U_3Si_2 dispersions are summarized in this report to facilitate the preparation and review of requests to use this fuel in research and test reactors.

2. PROPERTIES OF U_3Si_2 AND OTHER URANIUM SILICIDES

2.1 Uranium Silicide Phases

As is the case for uranium aluminide, uranium silicide normally consists of a mixture of intermetallic compounds, or phases. The quantity of each phase present depends upon the composition and homogeneity of the alloy and on its heat treatment. Since, as will be discussed later, the different uranium silicide phases behave differently under irradiation, knowledge of the phases to be expected in the fuel is necessary to correctly interpret the test results and to prepare specifications. A brief discussion of this topic follows; more detail can be found in Ref. 6.

The U-Si phase diagram is shown in Fig. 1. In the region of the phase diagram between 7.3 and 10.6 wt% Si, the two phases U_3Si_2 and USi exist, at equilibrium, in the proportions shown in Fig. 2. These two phases form directly upon cooling from the liquid state. The situation is more complicated for Si contents of less than 7.3 wt% because U_3Si is formed by a peritectoid (solid state) reaction. The as-cast alloy consists of primary U_3Si_2 with a

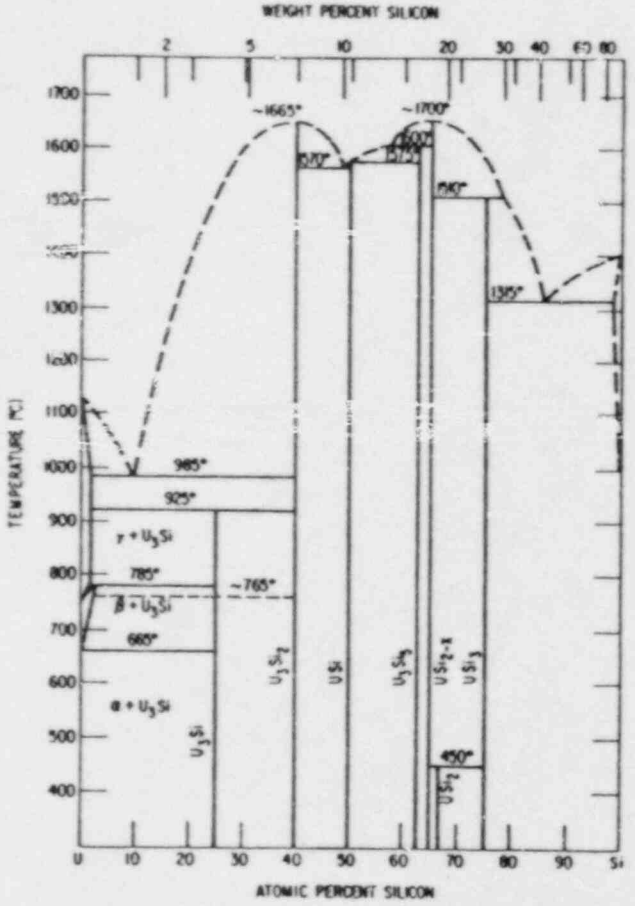

Fig. 1. The U-Si System.

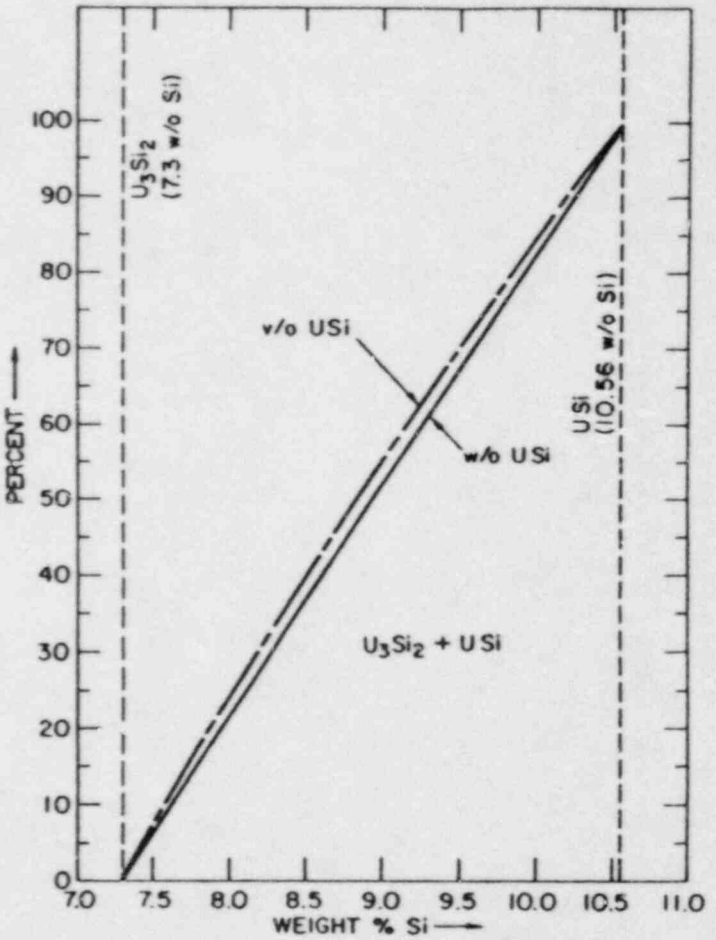

Fig. 2. Weight % (w/o) and Volume % (v/o) of USi vs. Weight % Si for Alloys at Equilibrium.

eutectic matrix of uranium solid solution (U_{ss}) and U_3Si_2. The proportions of U_3Si_2 and U_{ss} are shown in Fig. 3. Following prolonged heat treatment below the 925°C peritectoid temperature, U_{ss} reacts with U_3Si_2 to form U_3Si. Heat treatment of arc-cast ingots for 72 h at 800°C has been found to be sufficient to carry the reaction to completion. At equilibrium in the heat-treated alloy, the proportions of U_3Si and U_3Si_2 for Si contents between 3.9 and 7.3 wt% are shown in Fig. 4. Below 3.9 wt% Si the heat-treated alloy contains both U_3Si and U_{ss}.*

In practice it is essentially impossible to produce a perfectly homogeneous alloy at the exact stoichiometric composition of U_3Si_2 or to obtain equilibrium conditions. Therefore, the alloy can always be expected to contain two or more phases.† If the average composition is close to 7.3 wt%, local inhomogeneities may result in some regions of the as-cast alloy containing U_3Si_2 and USi and other regions containing U_3Si_2 and U_{ss}. If the alloy is then heat treated, the U_{ss} will be converted to U_3Si.

The practice at ANL has been to produce alloys slightly to the Si-rich side of U_3Si_2, typically 7.5 wt% Si, in order to minimize the possibility of the alloy containing measurable quantities of either U_{ss} or U_3Si. The U_3Si_2 irradiation tests discussed in this report have been obtained for fuels with Si contents ranging from ~7.2 to ~7.7 wt%. Some of the fuel was heat treated and some was used in the as-cast condition. The maximum amounts of secondary phases estimated to be present were 2 to 3 vol% of U_{ss}, 10 vol% of U_3Si, or 15 vol% of USi.

In this report and in other literature discussing uranium silicide-aluminum dispersion fuels, the convention is to use the name of the dominant phase for those alloys with average composition near that of the dominant phase. It must be remembered, however, that other minor phases will also be present and may contribute to the macroscopic behavior of the fuel.

2.2 Selected Physical and Mechanical Properties

Both U_3Si_2 and USi are brittle while U_3Si is tough and relatively soft. The measured hardness of U_3Si_2 was 742 DPH, compared to 265 DPH for U_3Si.[7]

---

*At its experimentally determined composition, 3.9 wt% Si, U_3Si actually contains 1.03 atoms of Si for every three atoms of U.

†The presence of impurities, which are not being considered here, complicates the situation further, since they may lead to the existence of still other phases.

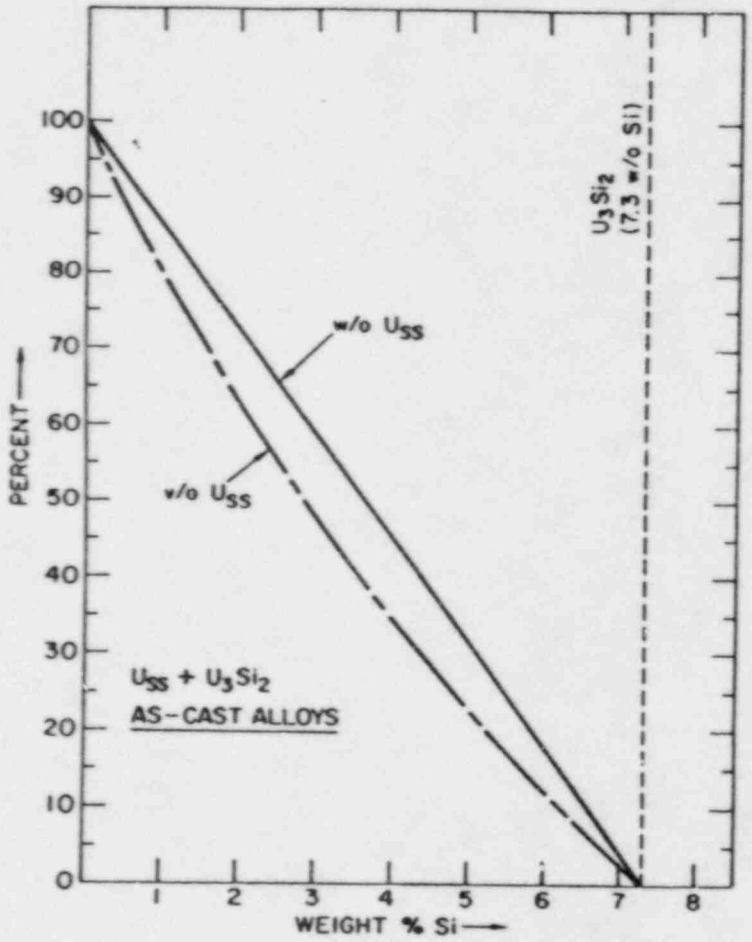

Fig. 3. Weight % (w/o) and Volume % (v/o) of Uranium Solid Solution (U_{SS}) vs. Weight % Si for As-Cast Alloys.

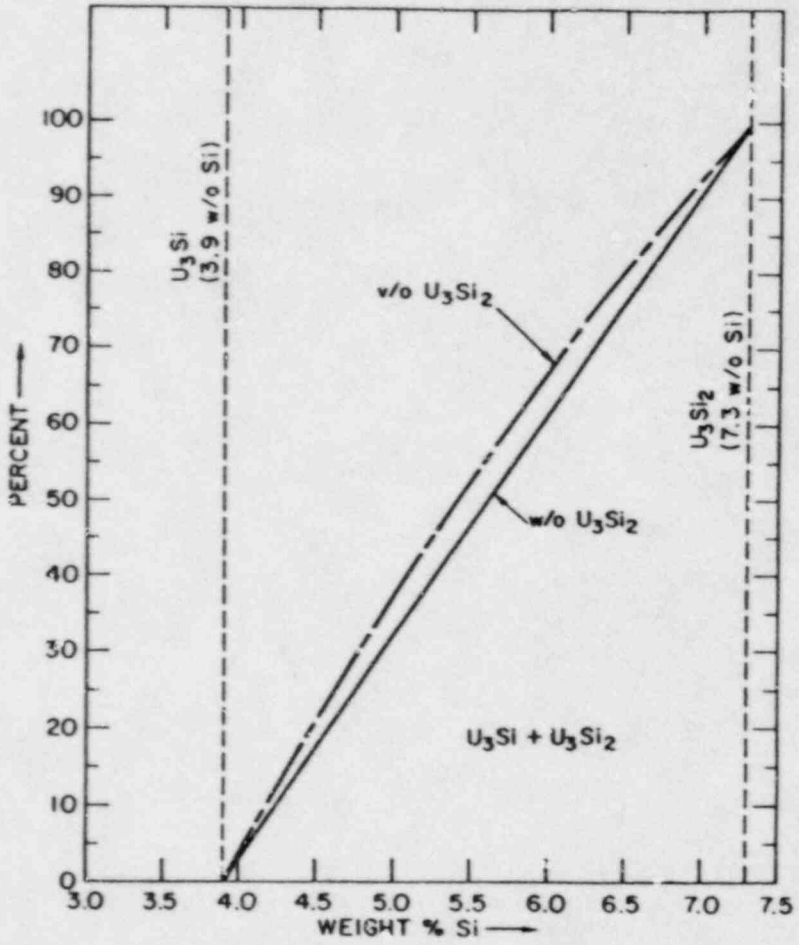

Fig. 4. Weight % (w/o) and Volume % (v/o) of U_3Si_2 vs. Weight % Si for Alloys at Equilibrium and Temperature <925°C.

The average thermal expansion coefficients of U_3Si_2 and U_3Si over the range 20 to 600°C are 15.2×10^{-6} and 15.8×10^{-6} per °C, respectively.[8]

A least squares quadratic fit of measured density vs. Si content for a series of depleted U-Si alloys with composition ranging from 4.0 to 7.5 wt% Si[7] and for USi[9] yields 12.2 and 15.4 Mg/m^3 for the densities of stoichiometric U_3Si_2 and U_3Si, respectively. For the fit the density of (depleted) USi was taken to be 10.86 Mg/m^3.[9] These densities are reduced by a negligible 0.2% for 20%-enriched uranium and by 1.1% for 93%-enriched uranium.

Both U_3Si_2 and U_3Si have a thermal conductivity of ~15 W/m·K.[8] Plots of specific heat data for stoichiometric U_3Si and for a U-Si alloy at 6.1 wt% Si are found in Ref. 10. From these data the specific heats of U_3Si_2 and U_3Si as a function of temperature (T, °C) have been derived:

$$C_p(U_3Si_2) = 199 + 0.104T \quad J/kg\cdot K \tag{1}$$

$$C_p(U_3Si) = 171 + 0.019T \quad J/kg\cdot K. \tag{2}$$

3. FUEL PLATE FABRICATION

3.1 Procedures

The procedures which have been used in fabricating U_3Si_2 fuel plates for irradiation tests are very similar to those already in use for UAl_x fuel. The procedures used at ANL to fabricate miniature fuel plates (miniplates) for irradiation testing are discussed in Ref. 11. Each of the commercial fabricators participating with the RERTR Program in the development and testing of U_3Si_2 fuel was encouraged to use its standard fabrication techniques and materials as much as was possible. A very brief general discussion of fabrication techniques follows.*

3.1.1 Fuel Powder

The uranium silicide alloys used in all of the irradiation tests were produced by melting uranium metal and elemental silicon in proper proportions in an arc furnace. The ingots were flipped and remelted from three to six times to produce a homogeneous material. Induction melting can also be used.

As discussed in Section 2.1, heat treatment (72 h at 800°C) is necessary only in those cases in which U_3Si is to be one of the end phases. In the

*A full set of procedures followed at ANL to produce miniplates is available on request from the authors.

early development work at ANL and, consequently, for the first U_3Si_2 ORR test elements produced by NUKEM* and CERCA,† the U_3Si_2 ingots were heat treated. The primary concern was that there be no U_{ss} present in the fuel plates. In later work, it was decided that heat treatment of U_3Si_2 ingots served no practical purpose, and, since it would add cost to commercial fabrication, the heat treatment step was eliminated. Hence, the fuel for all but the first four miniplates fabricated at ANL and for the ORR test elements produced by B&W** was not heat treated.

Both U_3Si_2 and USi are brittle and easily reduced to powder. In fact, the biggest concern is not to reduce the particle size too much. For the small volumes of powder needed at ANL, the U_3Si_2 was comminuted by hand using a steel mortar and pestle. Jaw crushers and/or hammer mills or ball mills were used by the commercial fabricators. Particle sizes ranged from <40 or <44 μm (fines), depending on whether metric or U.S. standard sieves were used, to 150 μm. The amount of fines in the irradiation test specimens ranged from 15 to 40 wt%. It should be noted that because of the brittle nature of U_3Si_2 and because of the high volume loading of fuel in high-density fuels, many of the larger fuel particles are broken during rolling, effectively increasing the number of fines. Uranium silicide is pyrophoric, and care must be taken when working with the powder in air. All fabricators conducted comminution in a glovebox with a neutral (N_2 or Ar) atmosphere. Average compositions and impurities of U_3Si_2 powders used to fabricate miniature plates and full-sized plates for irradiation testing are listed in Table I.

3.1.2 Fuel Plates

Fabrication of fuel plates followed the same procedures which had been established for UAl_x and U_3O_8 dispersion fuels. Fuel powder and aluminum powder were mixed in the desired proportions and formed under pressure into a powder-metallurgical compact. The compact was placed in the cavity of a "picture" frame, and cover plates to form the top and bottom cladding were welded in place to form a rolling billet. The billets were first hot rolled and then cold rolled to produce a plate of proper thickness. After hot rolling, a one-hour anneal at approximately the rolling temperature was conducted to test for the generation of blisters, indicating faulty bonding

---

*NUKEM GmbH, Hanau, Fed. Rep. of Germany.

†Compagnie pour l'Etude et la Réalisation de Combustibles Atomiques, Romans-sur-Isere, France.

**Babcock and Wilcox Company, Lynchburg, Virginia, U.S.A.

Table I. Reported Average U_3Si_2 Powder Compositions and Impurities

		Fabricator		
Major Constituent, wt%	ANL	B&W	CERCA	NUKEM
U	92.3	91.8 (91.2-92.3)	92.1	---
Si	7.5	7.4 (7.2- 7.7)	---	7.3
Impurity, ppm				
Al	26	4	---	400
B	---	5	<10	0.9
C	270	607	337	400
Cd	---	<0.5	<10	<5
Co	---	---	---	<5
Cu	---	7	---	96
Fe	96	6	---	550
H	6	---	13	---
Li	---	---	<5	<5
N	90	---	1672	---
Ni	---	5	---	---
O	429	806	1290	---
Zn	---	<2	---	<10

between cover and frame or between cover and fuel meat. Following shearing or machining to final size, the homogeneity of the uranium in the fuel meat was checked, either by real-time x-ray attenuation scanning or by densitometry of an x-radiograph. Full-sized plates for fuel elements were also inspected ultrasonically for areas of nonbond.

3.2 Special Considerations for High-Density U_3Si_2 Dispersion Fuel

Most of the fuel plates fabricated for irradiation testing contained between 40 and 50 vol% of fuel in the fuel meat, considerably in excess of the loadings of HEU dispersion fuels. Accordingly, special consideration must be given to certain fabrication procedures and/or specifications in order to achieve cost-effective yields of acceptable plates. The most important of these are briefly discussed below.

3.2.1 Dogbone

As the volume of fuel in the core increases, the core gets stronger. When the core is stronger than the frame and covers, the rolling process leaves the ends of the core thicker than the middle. A longitudinal cross section of the long, narrow fuel core with thickened ends resembles a bone, hence the name. A dogbone has two undesirable consequences: reduced cladding thickness and increased areal uranium density (the amount of uranium beneath a unit area of plate surface). The latter may result in excessively high surface heat fluxes during irradiation and be cause for rejection of the plate.

Two methods have been employed to reduce or eliminate "dogboning." If allowed by the specifications, a stronger aluminum alloy can be used for the frame and, possibly, the covers to more nearly match the strength of the fuel core. Of course, it is the strength at the rolling temperature (425 to 500°C) which is important. If the strength of the fuel core still exceeds the strength of available aluminum alloys, the ends of the compact can be tapered to compensate for the thickening at the ends of the rolled fuel core. Both methods have been successfully employed in producing high-density U_3Si_2 fuel plates for irradiation testing.

3.2.2 Minimum Cladding Thickness

As the volume loading of fuel particles increases so does the probability that fuel particles will come in contact with one another during rolling and that some will be projected into the cladding. Since the particle distribution in a dispersion fuel core is random, one cannot predict the location and depth of the penetrating particles.

Requirements for minimum cladding thickness in most specifications for HEU fuel plates date from the time of alloy cores. Once a proper set of rolling parameters had been determined for a fuel plate with an alloy core, the process was very repeatable. Core and cladding thickness could be reliably determined by examining a few metallographic sections of a few fuel plates. Unless a sophisticated and expensive device which can nondestructively measure the cladding thickness over single fuel particles is available, it is impossible to determine the actual minimum cladding thickness of a dispersion fuel plate. A statistical basis can be established for estimating minimum cladding thickness from the distribution of measured minima observed in metallographic sections of typical fuel plates.[12] Such a basis can be used to set acceptance criteria for the number of particles observed to penetrate to within a given distance of the cladding surface. One must always accept, however, the possibility that the cladding over some particles may be thinner than the stated minimum.

If a dogbone exists, there is a high probability that the point of minimum cladding exists in the dogbone region. Therefore, reducing the dogbone should increase the minimum cladding thickness. A reduction in the maximum allowed fuel particle size should decrease the penetration distance into the cladding, thereby increasing the minimum cladding thickness.

The minimum allowable cladding thickness for miniplates irradiated in the ORR was 0.20 mm. The minimum cladding thickness for full-sized fuel plates for use in test fuel elements was specified to be 0.25 mm; however, in some instances fuel plates were accepted from a batch exhibiting slightly smaller minima. No detrimental effects attributable to thin cladding were observed during testing.

3.2.3 Stray Fuel Particles

Another consequence of increased fuel loading is an increased number of fuel particles at the surface of the compact. Some of these exposed particles can be dislodged during assembly of the rolling billet or during rolling and deposited between the frame and covers--regions of the fuel plate which are supposed to be fuel free. The occurrence of stray fuel particles can be detected by examination of properly exposed x-radiographs, where the stray particles are seen as "white spots." Stray fuel particles are sources of both heat and fission products during irradiation. Unless the concentration of fuel particles is large, however, heat generation is small and of no practical consequence. Hence, the main concern is that the fuel particles not be in locations where they might become exposed to the coolant.

Table II. Thermal Conductivities of U_3Si_2-Aluminum Dispersions

Sample Identification	Fraction of Fuel -325M Mesh, wt%	Fuel Volume[1] Fraction, %	Porosity,[2] vol%	Thermal Conductivity of Dispersion at 60°C, W/m·K	Temperature Coefficient, $W/m \cdot K^2$
CS148	15	13.7	1.9	181	0.148
CS106	15	32.3	6.0	78	0.029
CS140	0	39.4	9.2	40	0.014
CS141	15	37.0	9.3	48	5×10^{-4}
CS142	25	39.1	9.5	40	0.017
CERCA #1	41.5	46.4	4.0	59	0.161
CERCA #2	41.5	46.4	4.0	59	0.076
CS143	15	46.4	15.4	13.9	0.010

[1]Determined on the thermal conductivity specimens using a radiographic technique.
[2]Average value for the roll-bonded fuel plate.

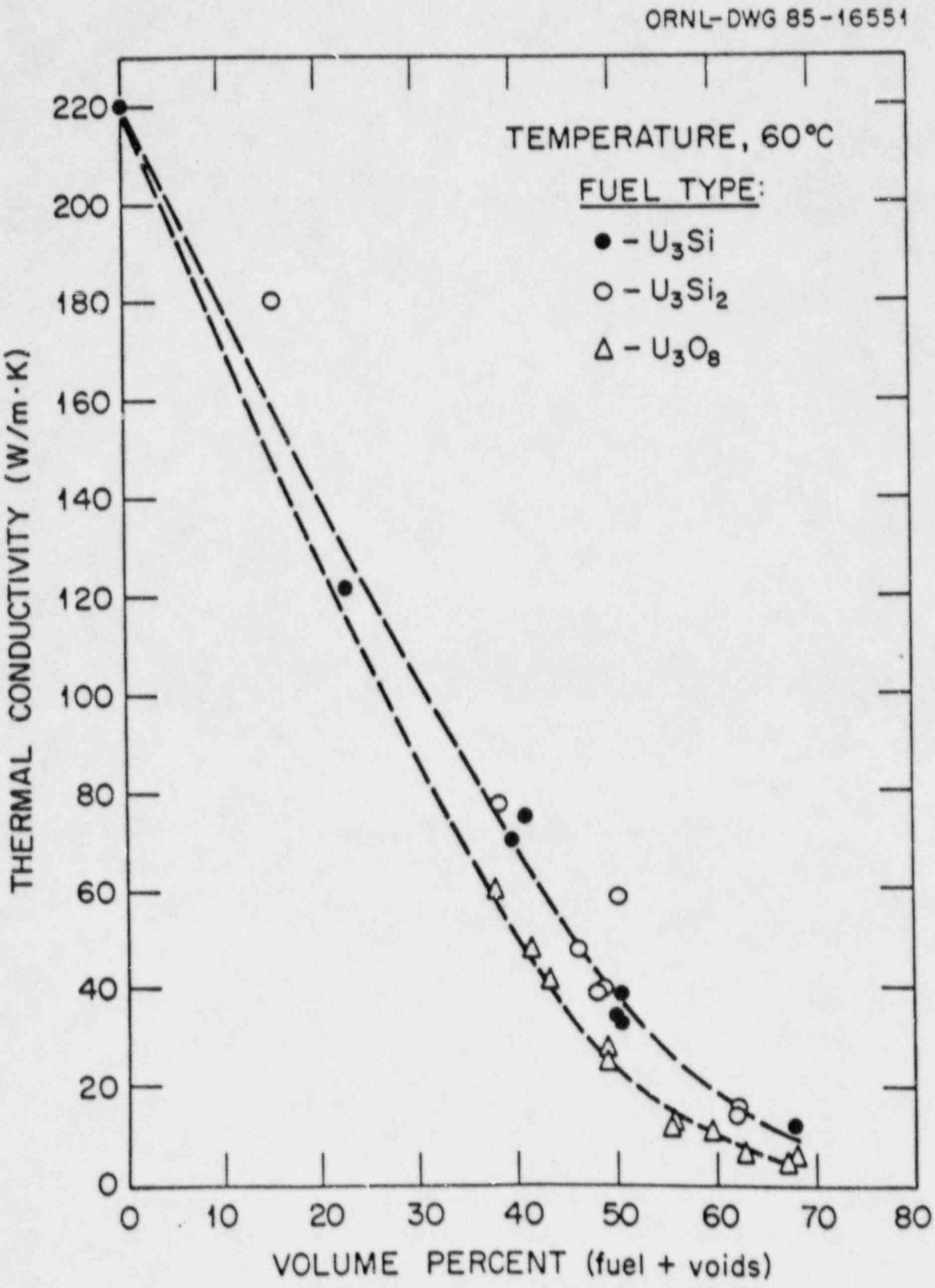

Fig. 6. Thermal Conductivities of Uranium Silicide- and U_3O_8-Aluminum Dispersion Fuels as a Function of Volume Fraction of Fuel Plus Voids (Porosity).

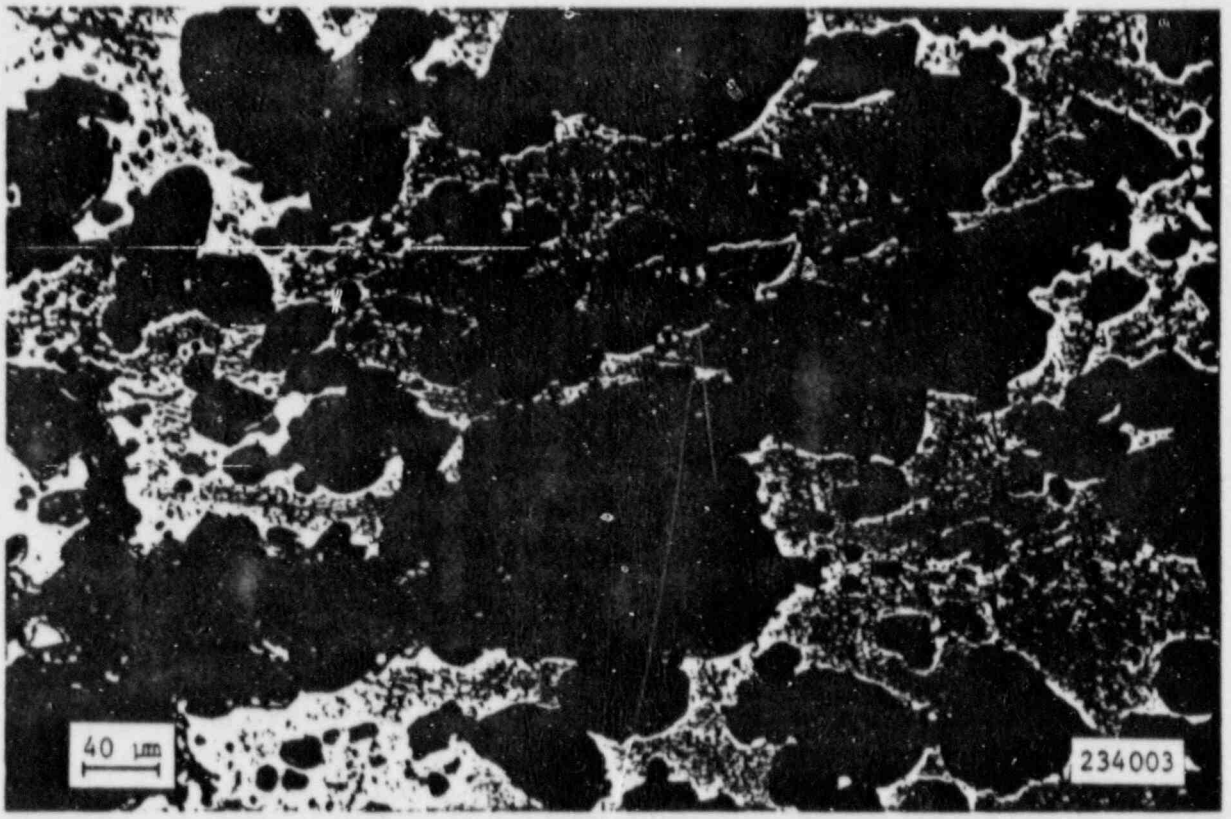

Fig. 12. Meat Microstructure of U_3Si Miniplate After 90% Bu.

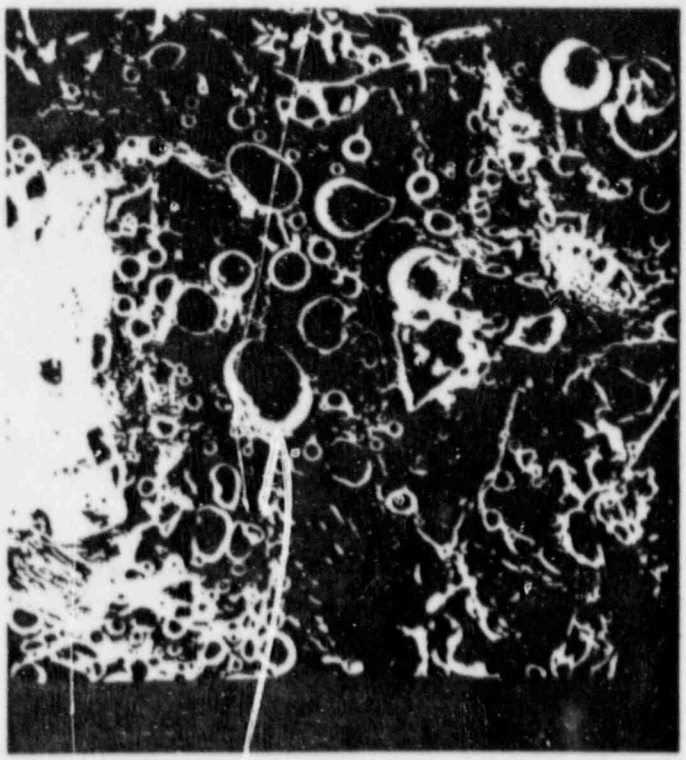

Fig. 13. Fission Gas Bubble Morphology in U_3Si After 90% Bu.

Table VI. Average Thickness Increase and Burnup of ORR U_3Si_2 Test Elements

Element No.	Low-Burnup End			Peak-Burnup Region			Element-Average Burnup, %
	Burnup, %	Thickness Increase, mils	μm	Burnup, %	Thickness Increase, mils	μm	
BSI-201	28	0	0	69	1.5	38	54
BSI-202	53	0	0	97	1.8	46	77
CSI-201	32	0.1	3	66	1.7	43	52
CSI-202	55	0.9	23	98	4.4	112	82
NSI-201	19	0.7	18	46	1.0	25	35
NSI-202	53	1.2	30	97	4.1	104	82

In conclusion, the metallographic observations are consistent with the relatively small plate thickness increases experienced during irradiation. The swelling is primarily caused by formation of two distinct fission gas bubble morphologies. The by-far-major phase, U_3Si_2, developed a very uniform and dense distribution of submicron-sized bubbles, characteristic of this fuel. The second silicide phase, U_3Si, which occurred in different amounts in the three fuels, developed its characteristic coarse, nonuniform bubble morphology. The amount of U_3Si and its larger swelling account, with the as-fabricated porosity, for the variability in overall plate swelling between plates of the different fabricators. The similarity of the average thickness changes in the high-burnup regions of elements CSI-202 and NSI-202 suggest that differences in bubble morphology may not be as great as comparison of Figs. 23 and 26 seems to indicate. Since only one section from the high-burnup region of CSI-202 was examined, there is a possibility that the section was atypical.

The non-U_3Si_2 phases present in the fuels are a result of fabrication practices. It is not possible, on a commercial scale, to produce a perfectly homogeneous alloy with the exact composition of a line compound such as U_3Si_2. Heat treatment of the ingots employed by CERCA and NUKEM but not by B&W would explain the absence of U_{ss} in the CERCA and NUKEM fuel. However, the U_{ss} phase found in B&W plates evidently reacted with aluminum during irradiation and had no deleterious effect on the swelling behavior of the fuel.

The minor differences in postirradiation microstructure of the fuel meat of the six ORR test elements reflect differences in fabrication practices of the manufacturers at the various times of fabrication. For example, when NUKEM fabricated the first two U_3Si_2 elements, it was not known that U_3Si behaved differently under irradiation than U_3Si_2 and that it might be desirable to control the amount of U_3Si in the fuel powder. Procedures developed during the course of U_3Si_2 development should result in a more uniform product now and in the future.

The discussion of this section has concentrated on differences in irradiation behavior in order to foster an understanding of the processes at work. However, the completely satisfactory behavior of the six U_3Si_2 test elements in the ORR, three of which were operated to ~80% burnup, must be emphasized.

5.2.3 Blister Threshold Temperature

The postirradiation blister threshold temperature has been used traditionally as an indicator of the relative failure resistance of plate-type dispersion fuels. The U_3Si_2 (and U_3Si) miniplates blistered at temperatures in the range of 515 to 530°C, except for very highly loaded U_3Si miniplates

which, at the threshold of breakaway swelling, blistered at 450 to 475°C. Thirteen plates from the full-sized elements were blister tested. Blister temperatures were in the range of 550 to 575°C. The blister threshold temperature appears to be insensitive both to burnup and to fuel volume loading. These temperatures are at least as high as those measured for highly enriched UAl_x and U_3O_8 dispersion fuels in use today.[33,35]

5.2.4 Fission Product Release

Over the years several studies of fission product release from plate-type reactor fuels have been done, first for plates with U-Al alloy meat and later for plates with UAl_x and U_3O_8 dispersion meats. Results of these experiments have been summarized in Refs. 36 and 37. As part of the development of high-density fuels under the RERTR Program, some fission product release measurements of limited scope have been performed.

Measurements using UAl_x miniplates were performed at ORNL in collaboration with the Kyoto University Research Reactor Institute primarily to determine the threshold temperature for fission product release and to measure release rates above that temperature.[38] These tests showed that the first significant release of gaseous fission products occurred when the fuel plate blistered. Another significant release occurred at about the solidus temperature of the cladding, and a third significant release occurred at about the UAl_4-Al eutectic temperature. Only very small releases of ^{131}I and ^{137}Cs were detected; however, since the system was designed primarily for the measurement of gaseous fission products, it is likely that only a small fraction of the total quantity released was detected.

Similar measurements, using the same equipment, were made using U_3O_8 and U_3Si miniplates, with similar results.[39] The first release of gaseous fission products was detected when the plates blistered, at 500°C for the U_3Si plate and at 550°C for the U_3O_8 plates. Essentially all of the gaseous fission products had been released by the end of the test at 650°C. From the amounts of Cs detected in the traps and from visual observations of deposits on the sample holder following the 650°C test, it was determined that much more Cs was released from the U_3Si plate than from the U_3O_8 plate.

It is expected that the fission product release characteristics of U_3Si_2 dispersed in aluminum are similar to those of U_3Si. The major release of fission gas occurred at about the aluminum melting temperature, where it is known from the DTA studies discussed in Section 4.5 that both U_3Si_2 and U_3Si fully react with the aluminum. The disruption of the fuel structure during the reaction undoubtedly enhances the release of the volatile and solid fission products. Release fractions in U_3Si_2 fuel might be less than those in U_3Si

4. F. Cherruau, "The Caramel Fuel in OSIRIS: The Complete Conversion of a High Flux Research Reactor to a Low Enriched Fuel," Proc. Int. Mtg. on Development, Fabrication and Application of Reduced Enrichment Fuels for Research and Test Reactors, Argonne, Illinois, November 12-14, 1980, Argonne National Laboratory Report ANL/RERTR/TM-3 (CONF-801144), pp. 310-318 (August 1983).

5. M. Barnier and J. P. Beylot, "OSIRIS, A MTR Adapted and Well Fitted to LEU Utilization Qualification and Development," Proc. Int. Mtg. on Reduced Enrichment for Research and Test Reactors, Tokai, Japan, October 24-27, 1983, Japan Atomic Energy Research Institute Report JAERI-M 84-073, pp. 256-267 (May 1984).

6. R. F. Domagala, "Phases in U-Si Alloys," Proc. 1986 Int. Mtg. on Reduced Enrichment for Research and Test Reactors, Gatlinburg, Tennessee, November 3-6, 1986, Argonne National Laboratory Report ANL/RERTR/TM-9, in press.

7. R. F. Domagala, T. C. Wiencek, and H. R. Thresh, "Some Properties of U-Si Alloys in the Composition Range U_3Si to U_3Si_2," Proc. 1984 Int. Mtg. on Reduced Enrichment for Research and Test Reactors, Argonne, Illinois, October 15-18, 1984, Argonne National Laboratory Report ANL/RERTR/TM-6 (CONF-8410173), pp. 47-60 (July 1985).

8. A. G. Samoilov, A. I. Kashtanov, and V. S. Volkov, *Dispersion-Fuel Nuclear Reactor Elements*, (1965), translated from the Russian by A. Aladjem, Israel Program for Scientific Translations Ltd., Jerusalem, pp. 54-57 (1968).

9. A. E. Dwight, "A Study of the Uranium-Aluminum-Silicon System," Argonne National Laboratory Report ANL-82-14, p. 29 (September 1982).

10. H. Shimizu, "The Properties and Irradiation Behavior of U_3Si_2," Atomics International Report NAA-SR-10621, p. 14 (July 25, 1965).

11. R. F. Domagala, T. C. Wiencek, and H. R. Thresh, "U-Si and U-Si-Al Dispersion Fuel Alloy Development for Research and Test Reactors," Nucl. Tech. 62, 353-360 (September 1983).

12. T. Görgenyi and U. Huth, "Determination of Cladding Thickness in Fuel Plates for Material Test and Research Reactors (MTR)," presented at Seminar on Research Reactor Operation and Use, Jülich, Fed. Rep. of Germany, September 14-18, 1981.

13. H. W. Hassel and E. Wehner, NUKEM, personal communication (April 1986).

14. G. Thamm, "The German AF-Program Status and Final Activities," Proc. 1986 Int. Mtg. on Reduced Enrichment for Research and Test Reactors, Gatlinburg, TN, November 3-6, 1986, Argonne National Laboratory Report ANL/RERTR/TM-9, in press.

15. K. Bogacik, "Status of LEU Programs at Babcock & Wilcox," *Reduced Enrichment for Research and Test Reactors--Proceedings of an International Meeting, Petten, The Netherlands, October 14-16, 1985*, P. von der Hardt and A. Travelli, Eds., D. Reidel Publishing Company, Dordrecht, pp. 165-173 (1986).

16. S. Nazaré, "Low Enrichment Dispersion Fuels for Research and Test Reactors," J. of Nucl. Materials 124, 14-24 (1984).

17. P. Toft and A. Jensen, "Differential Thermal Analysis and Metallographic Examinations of U_3Si_2 Powder and U_3Si_2/Al (38 w/o) Miniplates," *Reduced Enrichment for Research and Test Reactors--Proceedings of an International Meeting, Petten, The Netherlands, October 14-16, 1985*, P. von der Hardt and A. Travelli, Eds., D. Reidel Publishing Company, Dordrecht, pp. 373-381 (1986).

18. T. C. Wiencek, "A Study of the Effect of Fabrication Variables on the Quality of Fuel Plates," Proc. 1986 Int. Mtg. on Reduced Enrichment for Research and Test Reactors, Gatlinburg, Tennessee, November 3-6, 1986, Argonne National Laboratory Report ANL/RERTR/TM-9, in press.

19. *CRC Handbook of Chemistry and Physics*, 64th Edition, R. C. Weast, Ed., CRC Press, Boca Raton, pp. D-43 and D-44 (1983).

20. R. K. Williams, R. S. Graves, R. F. Domagala, and T. C. Wiencek, "Thermal Conductivities of U_3Si and U_3Si_2-Al Dispersion Fuels," Proc. 19th Int. Conf. on Thermal Conductivity, Cookeville, Tennessee, October 21-23, 1985, in press.

21. R. R. Hobbins, EG&G Idaho, unpublished information (1973).

22. G. L. Copeland and M. M. Martin, "Development of High-Uranium-Loaded U_3O_8-Al Fuel Plates," Nucl. Tech. 56, 547 (1982).

23. T. C. Wiencek, R. F. Domagala, and H. R. Thresh, "Thermal Compatibility Studies of Unirradiated Uranium Silicide Dispersed in Aluminum," Nucl. Tech. 71, 608-616 (1985).

24. C. E. Weber, "Progress on Dispersion Elements," *Progress in Nuclear Energy*, Ser. V, 2, Pergamon Press, N.Y. (1959).

25. R. F. Domagala, T. C. Wiencek, J. L. Snelgrove, M. I. Homa, and R. R. Heinrich, "Differential Thermal Analysis of U_3Si-Al and U_3Si_2-Al Reactions," Argonne National Laboratory Report ANL/RERTR/TM-7 (October 1984) and Am. Cer. Soc. Bull. 65(8), 1164-70 (1986).

26. S. Nazaré, "Reaction Behavior of U_xSi_y- and U_6Fe-Al Dispersions," Proc. 1984 Int. Mtg. on Reduced Enrichment for Research and Test Reactors, Argonne, Illinois, October 15-18, 1984, Argonne National Laboratory Report ANL/RERTR/TM-6 (Conf-8410173), pp. 39-46 (July 1985).

27. A. E. Pasto, G. L. Copeland, and M. M. Martin, "Quantitative Differential Thermal Analysis Study of the U_3O_8-Al Thermite Reaction," Am. Cer. Soc. Bull., 61(4), 491-496 (1982).

28. J. D. Fleming and J. W. Johnson, "Aluminum-U_3O_8 Exothermic Reactions," Nucleonics, 21(5), 84-87 (May 1963).

29. R. L. Senn and M. M. Martin, "Irradiation Testing of Miniature Fuel Plates for the RERTR Program," Oak Ridge National Laboratory Report ORNL/TM-7761 (July 1981).

30. G. L. Copeland, R. W. Hobbs, G. L. Hofman, and J. L. Snelgrove, "Performance of Low-Enriched U_3Si_2-Aluminum Dispersion Fuel Elements in the Oak Ridge Research Reactor," Argonne National Laboratory Report ANL/RERTR/TM-10 (October 1987).

31. C. Baas, M. Barnier, J. P. Beylot, P. Martel, and F. Merchie, "Progress Report on LEU Fuel Testing in CEA Reactors," Proc. 1986 Int. Mtg. on Reduced Enrichment for Research and Test Reactors, Gatlinburg, Tennessee, November 3-6, 1986, Argonne National Laboratory Report ANL/RERTR/TM-9, in press.

32. F. Merchie, CEN-G, personal communication (July 1987).

33. J. M. Beeston, R. R. Hobbins, G. W. Gibson, and W. C. Francis, "Development and Irradiation Performance of Uranium Aluminide Fuels in Test Reactors," Nucl. Tech. 49, 136-149 (June 1980).

34. G. L. Hofman, G. L. Copeland, and J. E. Sanecki, "Microscopic Investigation into the Irradiation Behavior of U_3O_8-Al Dispersion Fuel," Nucl. Tech. 72, 338-344 (1986).

35. A. E. Richt, R. W. Knight, and G. M. Adamson, Jr., "Postirradiation Examination and Evaluation of the Performance of HFIR Fuel Elements," Oak Ridge National Laboratory Report ORNL-4714 (December 1968).

36. D. Stahl, "Fuels for Research and Test Reactors, Status Review: July 1982," Argonne National Laboratory Report ANL-83-5, pp. 37-39 (December 1982).

37. R. E. Woodley, "The Release of Fission Products from Irradiated SRP Fuels at Elevated Temperature," Hanford Engineering Development Laboratory Report HEDL-7598 (June 1986).

38. T. Shibata, T. Tamai, M. Hayashi, J. C. Posey, and J. L. Snelgrove, "Release of Fission Products from Irradiated Aluminide Fuel at High Temperatures," Nucl. Sci. and Eng. 87, 405-417 (1984).

39. J. C. Posey, "Release of Fission Products from Miniature Fuel Plates at Elevated Temperatures," Proc. Int. Mtg. on Research and Test Reactor Core Conversions from HEU to LEU Fuels, Argonne, Illinois, November 8-10, 1982, Argonne National Laboratory Report ANL/RERTR/TM-4 (CONF-821155), pp. 117-133 (September 1983).

40. G. W. Parker, G. E. Creek, C. J. Barton, W. J. Martin, and R. A. Lorenz, "Out-of-Pile Studies of Fission-Product Release from Overheated Reactor Fuels at ORNL, 1955-1965," Oak Ridge National Laboratory Report ORNL-3981 (July 1967).

41. G. C. Rodrigues and A. P. Gouge, "Reprocessing RERTR Silicide Fuels," Savannah River Laboratory Report DP-1657 (May 1983).

42. U.S. Department of Energy, "Receipt and Financial Settlement Provisions for Nuclear Research Reactor Fuels," Federal Register 51(32), 5754-5756 (February 18, 1986) and Federal Register 51(42), 7487 (March 4, 1986).

DISTRIBUTION FOR ANL/RERTR/TM-11

Internal:

A. Schriesheim
C. E. Till
P. I. Amundson
L. Burris
D. W. Cissel
L. G. LeSage
R. A. Lewis
J. F. Marchaterre
R. J. Teunis
D. C. Wade
R. W. Weeks
A. Travelli (150)
J. L. Snelgrove (2)
R. F. Domagala (2)
G. L. Hofman (2)
F. J. Karasek
L. A. Neimark
D. R. Schmitt
H. R. Thresh
T. C. Wiencek (2)
ANL Contract File
ANL Patent Department
ANL Libraries (3)
TIS Files (6)

External:

DOE-TIC, for distribution per UC-83 (41)

Manager, Chicago Operations Office, DOE

Director, Technology Management Div., DOE-CH

J. P. Colton, ACDA
D. E. Bailey, DOE-NE
L. S. Rubenstein, NRC (2)
D. Stahl, SAI

ORNL:

E. D. Clemmer
G. L. Copeland (2)
R. W. Hobbs (2)
S. S. Hurt
R. W. Knight
D. L. Selby
R. L. Senn (2)
L. G. Shrader
J. H. Swanks
C. D. West

INEL:

K. R. Brown
R. E. Carter
C. H. Cooper
R. R. Hobbins
J. A. Lake
L. K. Seymour

C. Benjamin Alcock, The University of Toronto
Paul C. Shewmon, Ohio State University

Applied Physics Division Review Committee:

Paul W. Dickson, Jr., EG&G Idaho, Inc.
E. Linn Draper, Gulf State Utilities
Michael J. Driscoll, Massachusetts Institute of Technology
Robert L. Hellens, West Simsbury, Connecticut
William E. Kastenberg, University of California-L.A.
Daniel A. Meneley, University of New Brunswick
Warren F. Miller, Los Alamos National Laboratory

Changed Pages of ANL/RERTR/TM-11

Table of Contents

Table of Contents (Cont.)

List of Tables

The Use of U_3Si_2 Dispersed in Aluminum in Plate-Type Fuel Elements for Research and Test Reactors

1. INTRODUCTION

The U.S. Reduced Enrichment Research and Test Reactor (RERTR) Program was established by the U.S. Department of Energy in 1978 to provide the technical means to convert research and test reactors from the use of highly enriched uranium (HEU) fuel to the use of low-enriched uranium (LEU) fuel. In order to maintain the required excess reactivity of the reactor core, the amount of ^{235}U must be increased by 10 to 15% to overcome the additional neutron absorption of the greatly increased ^{238}U content in LEU fuel and the effects of a harder neutron spectrum. This additional ^{235}U and ^{238}U can be accommodated by increasing the uranium density of the fuel and/or by redesigning the fuel element to increase the volume fraction of fuel in the reactor core. The RERTR Program has vigorously pursued both paths with major efforts in fuel development and demonstration and in reactor analysis and design.[1]

Research and test reactor fuel elements consist of assemblies of fuel-containing plates or rods. The RERTR Program has concentrated its efforts on plate-type fuels since plate-type research and test reactors consume much more HEU than do rod-type reactors. High-density LEU rod-type fuels have been developed by GA Technologies for TRIGA reactors[2] and by Atomic Energy of Canada, Ltd.[3] Rod-type fuels will not be discussed further in this report.

The fuel plates used in the fuel elements for most research and test reactors consist of a fuel core, or "meat," in an aluminum alloy cladding. Originally, cast and wrought alloys of uranium and aluminum, consisting of UAl_3 and UAl_4 precipitates in an aluminum matrix, were used for the fuel meat. Fabrication of alloy cores with uranium densities above ~1.1 Mg U/m^3 is difficult, however, and powder metallurgical cores, with UAl_x (a combination of UAl_2, UAl_3, UAl_4, and Al phases) or U_3O_8 dispersed in aluminum, are now used in most cases. In 1978 the densest UAl_x fuel in use contained ~1.7 Mg U/m^3 in the fuel meat (~37 vol% UAl_x), and the densest U_3O_8 fuel in use contained ~1.3 Mg U/m^3 in the fuel meat (~18 vol% U_3O_8). The RERTR Program has developed and tested UAl_x and U_3O_8 dispersion fuels for LEU applications up to their practical fabrication limits--2.4 and 3.2 Mg U/m^3, respectively.

In order to minimize the need to redesign fuel elements to increase the fuel volume fraction and to make significant enrichment reductions in high-performance reactors even feasible, higher densities yet were needed. One approach, followed by the French Commissariat à l'Energie Atomique (CEA), utilized small wafers of sintered UO_2 contained in compartments of a fuel

plate produced by diffusion bonding Zircaloy frames, spacer wires, and cladding plates.[4] The 7%-enriched "caramel" fuel has performed well in OSIRIS;[5] however, fabricators of conventional plate-type fuels would have to implement a completely new fabrication process to produce caramel fuel.

The RERTR Program chose to pursue the use of high-density uranium-silicon alloys in place of UAl_x and U_3O_8 in conventional aluminum-matrix dispersion fuel in order to take advantage of the large commercial base of equipment for and experience in fabrication of such fuels. One uranium silicide compound, U_3Si_2, has been found to perform extremely well under irradiation and can provide a uranium density of at least 4.8 Mg/m^3.

The development and testing of uranium silicide fuels has been an international effort, involving other national reduced enrichment programs, several commercial fuel fabricators, and several test reactor operators. In particular, the testing of full-sized fuel elements has been performed cooperatively, with the U.S. Government providing the enriched uranium, the fuel fabricators providing the fabrication, and the U.S. Government or other governments providing the irradiations and postirradiation examinations.

Numerous results of the development and testing of uranium silicide-aluminum dispersion fuels have been published previously. The results for U_3Si_2 dispersions are summarized in this report to facilitate the preparation and review of requests to use this fuel in research and test reactors.

2. PROPERTIES OF U_3Si_2 AND OTHER URANIUM SILICIDES

2.1 Uranium Silicide Phases

As is the case for uranium aluminide, uranium silicide normally consists of a mixture of intermetallic compounds, or phases. The quantity of each phase present depends upon the composition and homogeneity of the alloy and on its heat treatment. Since, as will be discussed later, the different uranium silicide phases behave differently under irradiation, knowledge of the phases to be expected in the fuel is necessary to correctly interpret the test results and to prepare specifications. A brief discussion of this topic follows; more detail can be found in Ref. 6.

The U-Si phase diagram is shown in Fig. 1. In the region of the phase diagram between 7.3 and 10.6 wt% Si, the two phases U_3Si_2 and USi exist, at equilibrium, in the proportions shown in Fig. 2. These two phases form directly upon cooling from the liquid state. The situation is more complicated for Si contents of less than 7.3 wt% because U_3Si is formed by a peritectoid (solid state) reaction. The as-cast alloy consists of primary U_3Si_2 with a

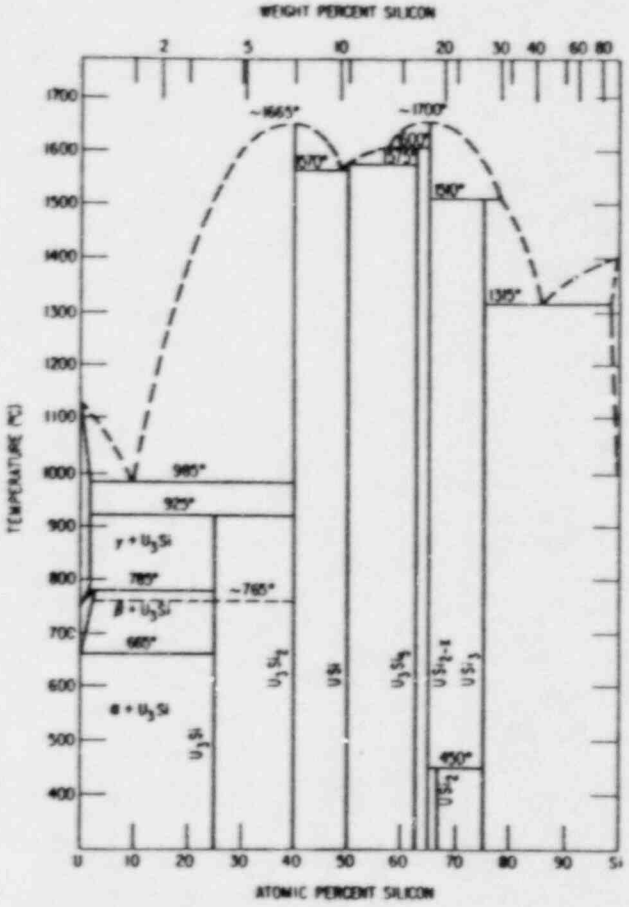

Fig. 1. The U-Si System.

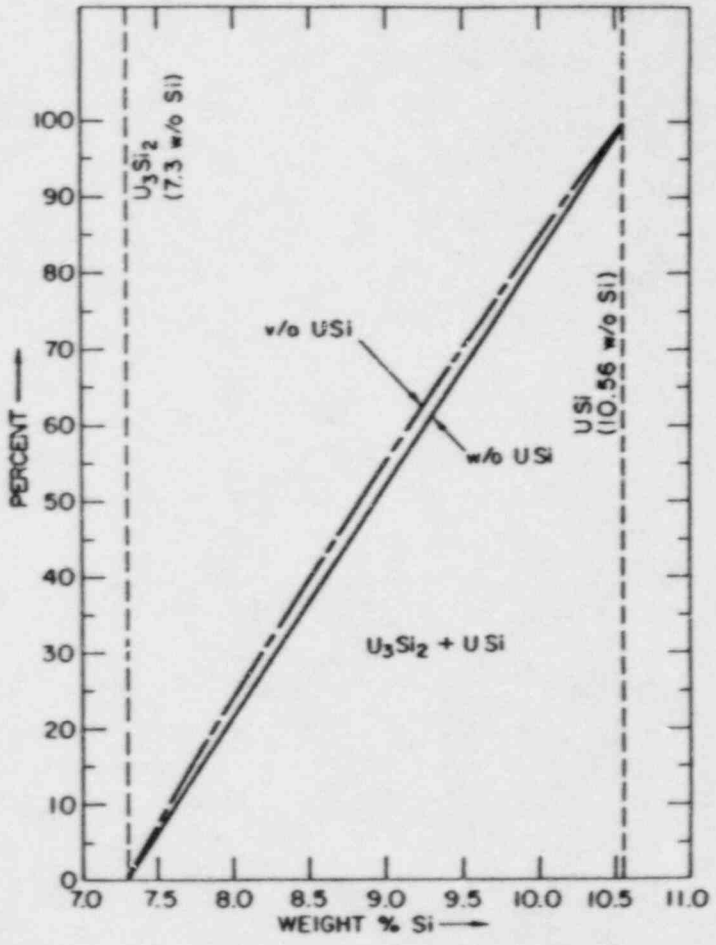

Fig. 2. Weight % (w/o) and Volume % (v/o) of USi vs. Weight % Si for Alloys at Equilibrium.

eutectic matrix of uranium solid solution (U_{ss}) and U_3Si_2. The proportions of U_3Si_2 and U_{ss} are shown in Fig. 3. Following prolonged heat treatment below the 925°C peritectoid temperature, U_{ss} reacts with U_3Si_2 to form U_3Si. Heat treatment of arc-cast ingots for 72 h at 800°C has been found to be sufficient to carry the reaction to completion. At equilibrium in the heat-treated alloy, the proportions of U_3Si and U_3Si_2 for Si contents between 3.9 and 7.3 wt% are shown in Fig. 4. Below 3.9 wt% Si the heat-treated alloy contains both U_3Si and U_{ss}.*

In practice it is essentially impossible to produce a perfectly homogeneous alloy at the exact stoichiometric composition of U_3Si_2 or to obtain equilibrium conditions. Therefore, the alloy can always be expected to contain two or more phases.† If the average composition is close to 7.3 wt%, local inhomogeneities may result in some regions of the as-cast alloy containing U_3Si_2 and USi and other regions containing U_3Si_2 and U_{ss}. If the alloy is then heat treated, the U_{ss} will be converted to U_3Si.

The practice at ANL has been to produce alloys slightly to the Si-rich side of U_3Si_2, typically 7.5 wt% Si, in order to minimize the possibility of the alloy containing measurable quantities of either U_{ss} or U_3Si. The U_3Si_2 irradiation tests discussed in this report have been obtained for fuels with Si contents ranging from ~7.2 to ~7.7 wt%. Some of the fuel was heat treated and some was used in the as-cast condition. The maximum amounts of secondary phases estimated to be present were 2 to 3 vol% of U_{ss}, 10 vol% of U_3Si, or 15 vol% of USi.

In this report and in other literature discussing uranium silicide-aluminum dispersion fuels, the convention is to use the name of the dominant phase for those alloys with average composition near that of the dominant phase. It must be remembered, however, that other minor phases will also be present and may contribute to the macroscopic behavior of the fuel.

2.2 Selected Physical and Mechanical Properties

Both U_3Si_2 and USi are brittle while U_3Si is tough and relatively soft. The measured hardness of U_3Si_2 was 742 DPH, compared to 265 DPH for U_3Si.[7]

---

*At its experimentally determined composition, 3.9 wt% Si, U_3Si actually contains 1.03 atoms of Si for every three atoms of U.

†The presence of impurities, which are not being considered here, complicates the situation further, since they may lead to the existence of still other phases.

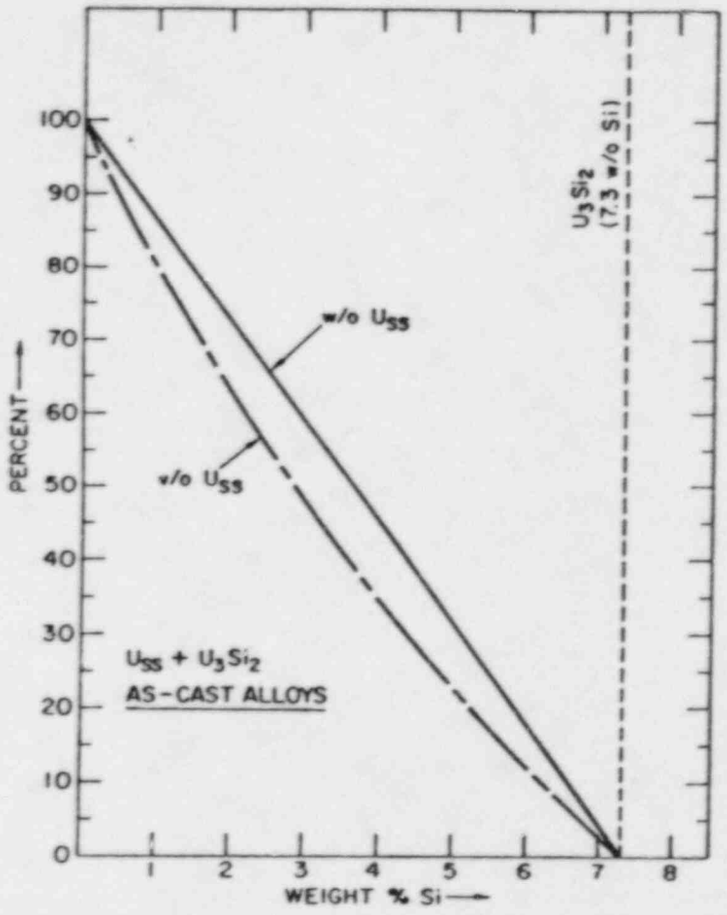

Fig. 3. Weight % (w/o) and Volume % (v/o) of Uranium Solid Solution (U_{SS}) vs. Weight % Si for As-Cast Alloys.

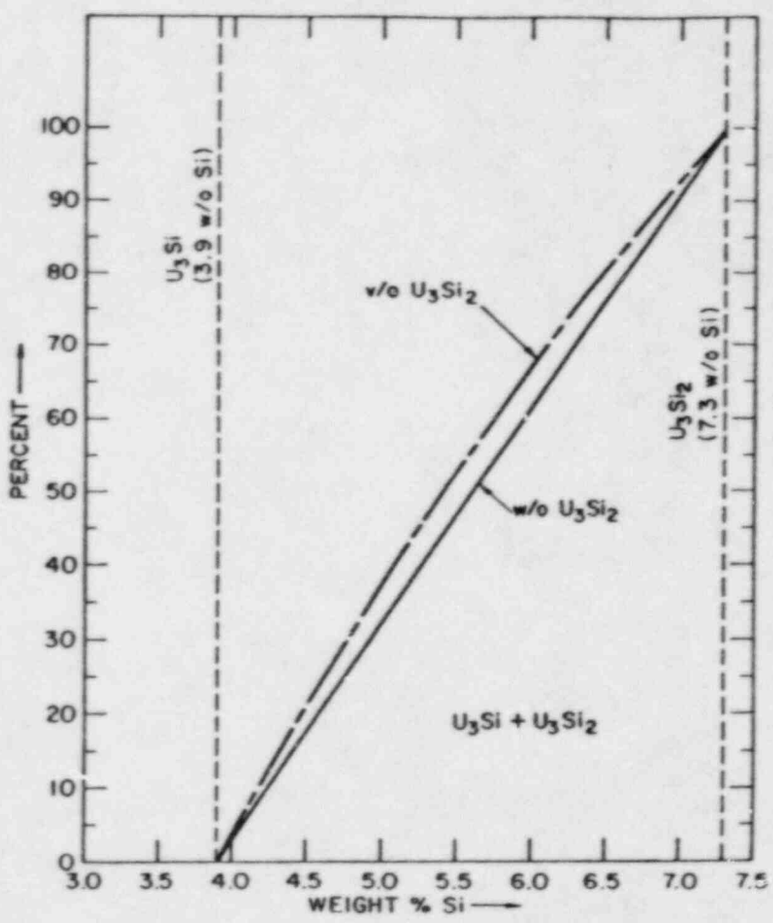

Fig. 4. Weight % (w/o) and Volume % (v/o) of U_3Si_2 vs. Weight % Si for Alloys at Equilibrium and Temperature <925°C.

The average thermal expansion coefficients of U_3Si_2 and U_3Si over the range 20 to 600°C are 15.2×10^{-6} and 15.8×10^{-6} per °C, respectively.[8]

A least squares quadratic fit of measured density vs. Si content for a series of depleted U-Si alloys with composition ranging from 4.0 to 7.5 wt% Si[7] and for USi[9] yields 12.2 and 15.4 Mg/m^3 for the densities of stoichiometric U_3Si_2 and U_3Si, respectively. For the fit the density of (depleted) USi was taken to be 10.86 Mg/m^3.[9] These densities are reduced by a negligible 0.2% for 20%-enriched uranium and by 1.1% for 93%-enriched uranium.

Both U_3Si_2 and U_3Si have a thermal conductivity of ~15 W/m·K.[8] Plots of specific heat data for stoichiometric U_3Si and for a U-Si alloy at 6.1 wt% Si are found in Ref. 10. From these data the specific heats of U_3Si_2 and U_3Si as a function of temperature (T, °C) have been derived:

$$C_p(U_3Si_2) = 199 + 0.104T \quad J/kg\cdot K \qquad (1)$$

$$C_p(U_3Si) = 171 + 0.019T \quad J/kg\cdot K. \qquad (2)$$

3. FUEL PLATE FABRICATION

3.1 Procedures

The procedures which have been used in fabricating U_3Si_2 fuel plates for irradiation tests are very similar to those already in use for UAl_x fuel. The procedures used at ANL to fabricate miniature fuel plates (miniplates) for irradiation testing are discussed in Ref. 11. Each of the commercial fabricators participating with the RERTR Program in the development and testing of U_3Si_2 fuel was encouraged to use its standard fabrication techniques and materials as much as was possible. A very brief general discussion of fabrication techniques follows.*

3.1.1 Fuel Powder

The uranium silicide alloys used in all of the irradiation tests were produced by melting uranium metal and elemental silicon in proper proportions in an arc furnace. The ingots were flipped and remelted from three to six times to produce a homogeneous material. Induction melting can also be used.

As discussed in Section 2.1, heat treatment (72 h at 800°C) is necessary only in those cases in which U_3Si is to be one of the end phases. In the

*A full set of procedures followed at ANL to produce miniplates is available on request from the authors.

early development work at ANL and, consequently, for the first U_3Si_2 ORR test elements produced by NUKEM* and CERCA,† the U_3Si_2 ingots were heat treated. The primary concern was that there be no U_{ss} present in the fuel plates. In later work, it was decided that heat treatment of U_3Si_2 ingots served no practical purpose, and, since it would add cost to commercial fabrication, the heat treatment step was eliminated. Hence, the fuel for all but the first four miniplates fabricated at ANL and for the ORR test elements produced by B&W** was not heat treated.

Both U_3Si_2 and USi are brittle and easily reduced to powder. In fact, the biggest concern is not to reduce the particle size too much. For the small volumes of powder needed at ANL, the U_3Si_2 was comminuted by hand using a steel mortar and pestle. Jaw crushers and/or hammer mills or ball mills were used by the commercial fabricators. Particle sizes ranged from <40 or <44 μm (fines), depending on whether metric or U.S. standard sieves were used, to 150 μm. The amount of fines in the irradiation test specimens ranged from 15 to 40 wt%. It should be noted that because of the brittle nature of U_3Si_2 and because of the high volume loading of fuel in high-density fuels, many of the larger fuel particles are broken during rolling, effectively increasing the number of fines. Uranium silicide is pyrophoric, and care must be taken when working with the powder in air. All fabricators conducted comminution in a glovebox with a neutral (N_2 or Ar) atmosphere. Average compositions and impurities of U_3Si_2 powders used to fabricate miniature plates and full-sized plates for irradiation testing are listed in Table 1.

3.1.2 Fuel Plates

Fabrication of fuel plates followed the same procedures which had been established for UAl_x and U_3O_8 dispersion fuels. Fuel powder and aluminum powder were mixed in the desired proportions and formed under pressure into a powder-metallurgical compact. The compact was placed in the cavity of a "picture" frame, and cover plates to form the top and bottom cladding were welded in place to form a rolling billet. The billets were first hot rolled and then cold rolled to produce a plate of proper thickness. After hot rolling, a one-hour anneal at approximately the rolling temperature was conducted to test for the generation of blisters, indicating faulty bonding

---

*NUKEM GmbH, Hanau, Fed. Rep. of Germany.

†Compagnie pour l'Etude et la Réalisation de Combustibles Atomiques, Romans-sur-Isere, France.

**Babcock and Wilcox Company, Lynchburg, Virginia, U.S.A.

Table I. Reported Average U_3Si_2 Powder Compositions and Impurities

		Fabricator		
Major Constituent, wt%	ANL	B&W	CERCA	NUKEM
U	92.3	91.8 (91.2-92.3)	92.1	---
Si	7.5	7.4 (7.2- 7.7)	---	7.3
Impurity, ppm				
Al	26	4	---	400
B	---	5	<10	0.9
C	270	607	337	400
Cd	---	<0.5	<10	<5
Co	---	---	---	<5
Cu	---	7	---	96
Fe	96	6	---	550
H	6	---	13	---
Li	---	---	<5	<5
N	90	---	1672	---
Ni	---	5	---	---
O	429	806	1290	---
Zn	---	<2	---	<10

between cover and frame or between cover and fuel meat. Following shearing or machining to final size, the homogeneity of the uranium in the fuel meat was checked, either by real-time x-ray attenuation scanning or by densitometry of an x-radiograph. Full-sized plates for fuel elements were also inspected ultrasonically for areas of nonbond.

3.2 Special Considerations for High-Density U_3Si_2 Dispersion Fuel

Most of the fuel plates fabricated for irradiation testing contained between 40 and 50 vol% of fuel in the fuel meat, considerably in excess of the loadings of HEU dispersion fuels. Accordingly, special consideration must be given to certain fabrication procedures and/or specifications in order to achieve cost-effective yields of acceptable plates. The most important of these are briefly discussed below.

3.2.1 Dogbone

As the volume of fuel in the core increases, the core gets stronger. When the core is stronger than the frame and covers, the rolling process leaves the ends of the core thicker than the middle. A longitudinal cross section of the long, narrow fuel core with thickened ends resembles a bone, hence the name. A dogbone has two undesirable consequences: reduced cladding thickness and increased areal uranium density (the amount of uranium beneath a unit area of plate surface). The latter may result in excessively high surface heat fluxes during irradiation and be cause for rejection of the plate.

Two methods have been employed to reduce or eliminate "dogboning." If allowed by the specifications, a stronger aluminum alloy can be used for the frame and, possibly, the covers to more nearly match the strength of the fuel core. Of course, it is the strength at the rolling temperature (425 to 500°C) which is important. If the strength of the fuel core still exceeds the strength of available aluminum alloys, the ends of the compact can be tapered to compensate for the thickening at the ends of the rolled fuel core. Both methods have been successfully employed in producing high-density U_3Si_2 fuel plates for irradiation testing.

3.2.2 Minimum Cladding Thickness

As the volume loading of fuel particles increases so does the probability that fuel particles will come in contact with one another during rolling and that some will be projected into the cladding. Since the particle distribution in a dispersion fuel core is random, one cannot predict the location and depth of the penetrating particles.

Requirements for minimum cladding thickness in most specifications for HEU fuel plates date from the time of alloy cores. Once a proper set of rolling parameters had been determined for a fuel plate with an alloy core, the process was very repeatable. Core and cladding thickness could be reliably determined by examining a few metallographic sections of a few fuel plates. Unless a sophisticated and expensive device which can nondestructively measure the cladding thickness over single fuel particles is available, it is impossible to determine the actual minimum cladding thickness of a dispersion fuel plate. A statistical basis can be established for estimating minimum cladding thickness from the distribution of measured minima observed in metallographic sections of typical fuel plates.[12] Such a basis can be used to set acceptance criteria for the number of particles observed to penetrate to within a given distance of the cladding surface. One must always accept, however, the possibility that the cladding over some particles may be thinner than the stated minimum.

If a dogbone exists, there is a high probability that the point of minimum cladding exists in the dogbone region. Therefore, reducing the dogbone should increase the minimum cladding thickness. A reduction in the maximum allowed fuel particle size should decrease the penetration distance into the cladding, thereby increasing the minimum cladding thickness.

The minimum allowable cladding thickness for miniplates irradiated in the ORR was 0.20 mm. The minimum cladding thickness for full-sized fuel plates for use in test fuel elements was specified to be 0.25 mm; however, in some instances fuel plates were accepted from a batch exhibiting slightly smaller minima. No detrimental effects attributable to thin cladding were observed during testing.

3.2.3 Stray Fuel Particles

Another consequence of increased fuel loading is an increased number of fuel particles at the surface of the compact. Some of these exposed particles can be dislodged during assembly of the rolling billet or during rolling and deposited between the frame and covers--regions of the fuel plate which are supposed to be fuel free. The occurrence of stray fuel particles can be detected by examination of properly exposed x-radiographs, where the stray particles are seen as "white spots." Stray fuel particles are sources of both heat and fission products during irradiation. Unless the concentration of fuel particles is large, however, heat generation is small and of no practical consequence. Hence, the main concern is that the fuel particles not be in locations where they might become exposed to the coolant.

Table II. Thermal Conductivities of U_3Si_2-Aluminum Dispersions

Sample Identification	Fraction of Fuel -325M Mesh, wt%	Fuel Volume[1] Fraction, %	Porosity,[2] vol%	Thermal Conductivity of Dispersion at 60°C, W/m•K	Temperature Coefficient, W/m•K[2]
CS148	15	13.7	1.9	181	0.148
CS106	15	32.3	6.0	78	0.029
CS140	0	39.4	9.2	40	0.014
CS141	15	37.0	9.3	48	5×10^{-4}
CS142	25	39.1	9.5	40	0.017
CERCA #1	41.5	46.4	4.0	59	0.161
CERCA #2	41.5	46.4	4.0	59	0.076
CS143	15	46.4	15.4	13.9	0.010

[1]Determined on the thermal conductivity specimens using a radiographic technique.
[2]Average value for the roll-bonded fuel plate.

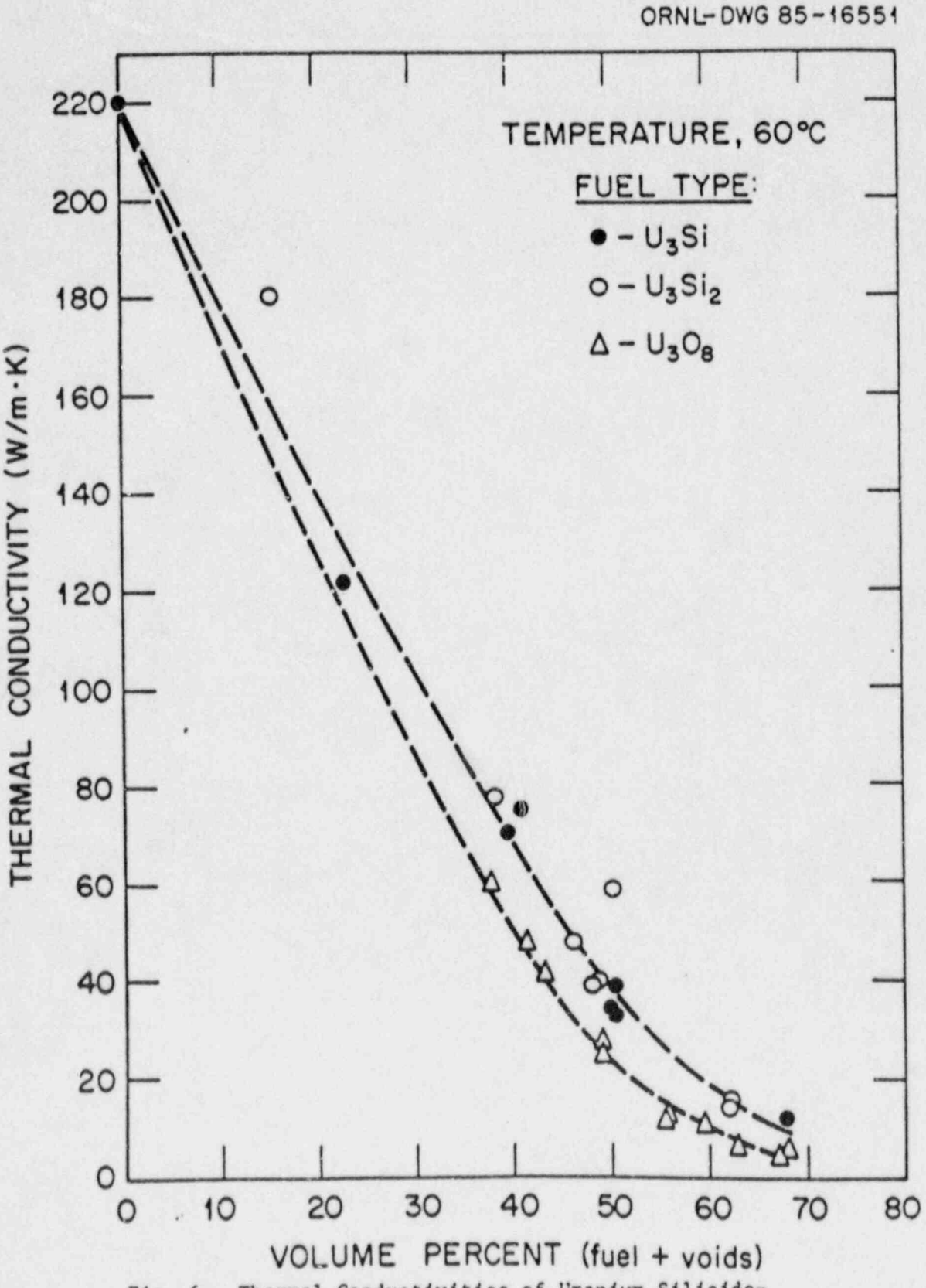

Fig. 6. Thermal Conductivities of Uranium Silicide- and U_3O_8-Aluminum Dispersion Fuels as a Function of Volume Fraction of Fuel Plus Voids (Porosity).

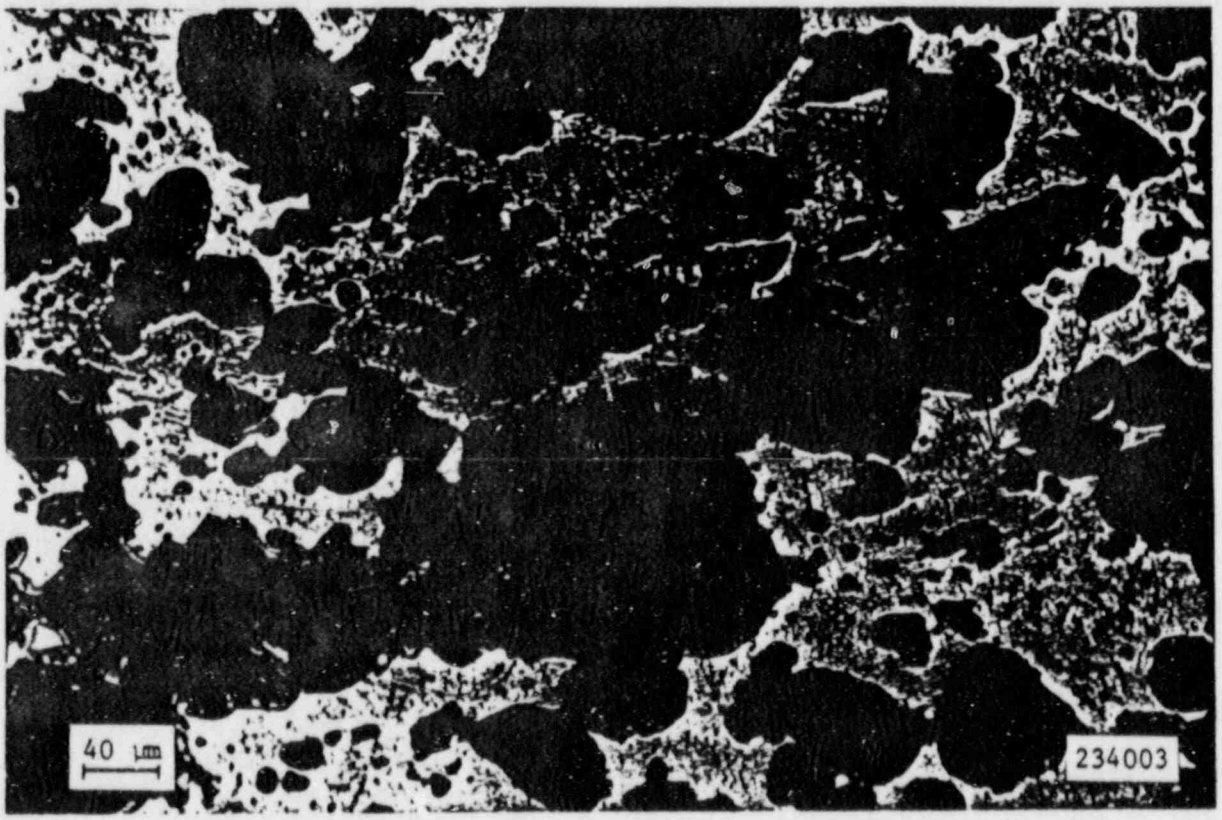

Fig. 12. Meat Microstructure of U_3Si Miniplate After 90% Bu.

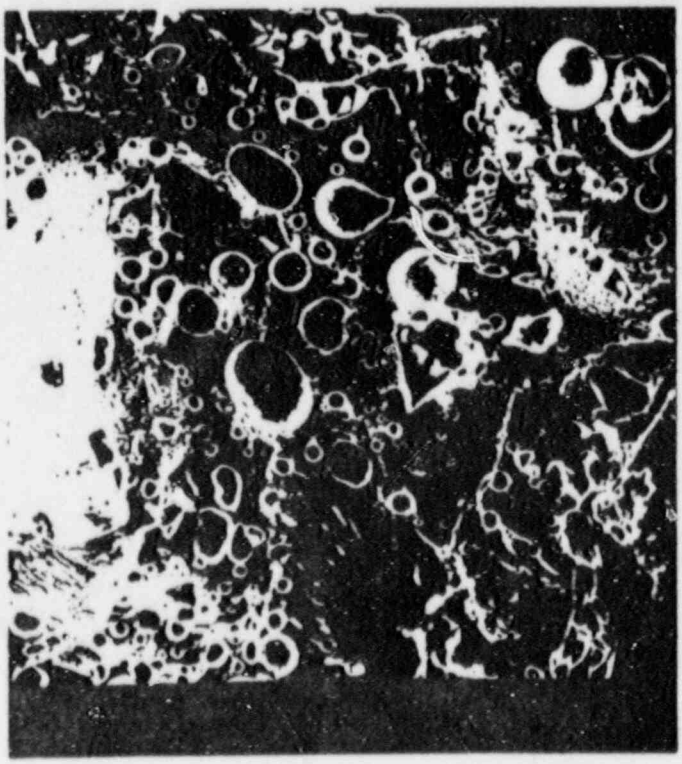

Fig. 13. Fission Gas Bubble Morphology in U_3Si After 90% Bu.

Table VI. Average Thickness Increase and Burnup of ORR U_3Si_2 Test Elements

Element No.	Low-Burnup End			Peak-Burnup Region			Element-Average Burnup, %
	Burnup, %	Thickness Increase, mils	µm	Burnup, %	Thickness Increase, mils	µm	
BSI-201	28	0	0	69	1.5	38	54
BSI-202	53	0	0	97	1.8	46	77
CSI-201	32	0.1	3	66	1.7	43	52
CSI-202	55	0.9	23	98	4.4	112	82
NSI-201	19	0.7	18	46	1.0	25	35
NSI-202	53	1.2	30	97	4.1	104	82

In conclusion, the metallographic observations are consistent with the relatively small plate thickness increases experienced during irradiation. The swelling is primarily caused by formation of two distinct fission gas bubble morphologies. The by-far-major phase, U_3Si_2, developed a very uniform and dense distribution of submicron-sized bubbles, characteristic of this fuel. The second silicide phase, U_3Si, which occurred in different amounts in the three fuels, developed its characteristic coarse, nonuniform bubble morphology. The amount of U_3Si and its larger swelling account, with the as-fabricated porosity, for the variability in overall plate swelling between plates of the different fabricators. The similarity of the average thickness changes in the high-burnup regions of elements CSI-202 and NSI-202 suggest that differences in bubble morphology may not be as great as comparison of Figs. 23 and 26 seems to indicate. Since only one section from the high-burnup region of CSI-202 was examined, there is a possibility that the section was atypical.

The non-U_3Si_2 phases present in the fuels are a result of fabrication practices. It is not possible, on a commercial scale, to produce a perfectly homogeneous alloy with the exact composition of a line compound such as U_3Si_2. Heat treatment of the ingots employed by CERCA and NUKEM but not by B&W would explain the absence of U_{ss} in the CERCA and NUKEM fuel. However, the U_{ss} phase found in B&W plates evidently reacted with aluminum during irradiation and had no deleterious effect on the swelling behavior of the fuel.

The minor differences in postirradiation microstructure of the fuel meat of the six ORR test elements reflect differences in fabrication practices of the manufacturers at the various times of fabrication. For example, when NUKEM fabricated the first two U_3Si_2 elements, it was not known that U_3Si behaved differently under irradiation than U_3Si_2 and that it might be desirable to control the amount of U_3Si in the fuel powder. Procedures developed during the course of U_3Si_2 development should result in a more uniform product now and in the future.

The discussion of this section has concentrated on differences in irradiation behavior in order to foster an understanding of the processes at work. However, the completely satisfactory behavior of the six U_3Si_2 test elements in the ORR, three of which were operated to ~80% burnup, must be emphasized.

5.2.3 Blister Threshold Temperature

The postirradiation blister threshold temperature has been used traditionally as an indicator of the relative failure resistance of plate-type dispersion fuels. The U_3Si_2 (and U_3Si) miniplates blistered at temperatures in the range of 515 to 530°C, except for very highly loaded U_3Si miniplates

which, at the threshold of breakaway swelling, blistered at 450 to 475°C. Thirteen plates from the full-sized elements were blister tested. Blister temperatures were in the range of 550 to 575°C. The blister threshold temperature appears to be insensitive both to burnup and to fuel volume loading. These temperatures are at least as high as those measured for highly enriched UAl_x and U_3O_8 dispersion fuels in use today.[33,35]

5.2.4 Fission Product Release

Over the years several studies of fission product release from plate-type reactor fuels have been done, first for plates with U-Al alloy meat and later for plates with UAl_x and U_3O_8 dispersion meats. Results of these experiments have been summarized in Refs. 36 and 37. As part of the development of high-density fuels under the RERTR Program, some fission product release measurements of limited scope have been performed.

Measurements using UAl_x miniplates were performed at ORNL in collaboration with the Kyoto University Research Reactor Institute primarily to determine the threshold temperature for fission product release and to measure release rates above that temperature.[38] These tests showed that the first significant release of gaseous fission products occurred when the fuel plate blistered. Another significant release occurred at about the solidus temperature of the cladding, and a third significant release occurred at about the UAl_4-Al eutectic temperature. Only very small releases of ^{131}I and ^{137}Cs were detected; however, since the system was designed primarily for the measurement of gaseous fission products, it is likely that only a small fraction of the total quantity released was detected.

Similar measurements, using the same equipment, were made using U_3O_8 and U_3Si miniplates, with similar results.[39] The first release of gaseous fission products was detected when the plates blistered, at 500°C for the U_3Si plate and at 550°C for the U_3O_8 plates. Essentially all of the gaseous fission products had been released by the end of the test at 650°C. From the amounts of Cs detected in the traps and from visual observations of deposits on the sample holder following the 650°C test, it was determined that much more Cs was released from the U_3Si plate than from the U_3O_8 plate.

It is expected that the fission product release characteristics of U_3Si_2 dispersed in aluminum are similar to those of U_3Si. The major release of fission gas occurred at about the aluminum melting temperature, where it is known from the DTA studies discussed in Section 4.5 that both U_3Si_2 and U_3Si fully react with the aluminum. The disruption of the fuel structure during the reaction undoubtedly enhances the release of the volatile and solid fission products. Release fractions in U_3Si_2 fuel might be less than those in U_3Si

4. F. Cherruau, "The Caramel Fuel in OSIRIS: The Complete Conversion of a High Flux Research Reactor to a Low Enriched Fuel," Proc. Int. Mtg. on Development, Fabrication and Application of Reduced Enrichment Fuels for Research and Test Reactors, Argonne, Illinois, November 12-14, 1980, Argonne National Laboratory Report ANL/RERTR/TM-3 (CONF-801144), pp. 310-318 (August 1983).

5. M. Barnier and J. P. Beylot, "OSIRIS, A MTR Adapted and Well Fitted to LEU Utilization Qualification and Development," Proc. Int. Mtg. on Reduced Enrichment for Research and Test Reactors, Tokai, Japan, October 24-27, 1983, Japan Atomic Energy Research Institute Report JAERI-M 84-073, pp. 256-267 (May 1984).

6. R. F. Domagala, "Phases in U-Si Alloys," Proc. 1986 Int. Mtg. on Reduced Enrichment for Research and Test Reactors, Gatlinburg, Tennessee, November 3-6, 1986, Argonne National Laboratory Report ANL/RERTR/TM-9, in press.

7. R. F. Domagala, T. C. Wiencek, and H. R. Thresh, "Some Properties of U-Si Alloys in the Composition Range U_3Si to U_3Si_2," Proc. 1984 Int. Mtg. on Reduced Enrichment for Research and Test Reactors, Argonne, Illinois, October 15-18, 1984, Argonne National Laboratory Report ANL/RERTR/TM-6 (CONF-8410173), pp. 47-60 (July 1985).

8. A. G. Samoilov, A. I. Kashtanov, and V. S. Volkov, *Dispersion-Fuel Nuclear Reactor Elements*, (1965), translated from the Russian by A. Aladjem, Israel Program for Scientific Translations Ltd., Jerusalem, pp. 54-57 (1968).

9. A. E. Dwight, "A Study of the Uranium-Aluminum-Silicon System," Argonne National Laboratory Report ANL-82-14, p. 29 (September 1982).

10. H. Shimizu, "The Properties and Irradiation Behavior of U_3Si_2," Atomics International Report NAA-SR-10621, p. 14 (July 25, 1965).

11. R. F. Domagala, T. C. Wiencek, and H. R. Thresh, "U-Si and U-Si-Al Dispersion Fuel Alloy Development for Research and Test Reactors," Nucl. Tech. 62, 353-360 (September 1983).

12. T. Görgenyi and U. Huth, "Determination of Cladding Thickness in Fuel Plates for Material Test and Research Reactors (MTR)," presented at Seminar on Research Reactor Operation and Use, Jülich, Fed. Rep. of Germany, September 14-18, 1981.

13. H. W. Hassel and E. Wehner, NUKEM, personal communication (April 1986).

14. G. Thamm, "The German AF-Program Status and Final Activities," Proc. 1986 Int. Mtg. on Reduced Enrichment for Research and Test Reactors, Gatlinburg, TN, November 3-6, 1986, Argonne National Laboratory Report ANL/RERTR/TM-9, in press.

15. K. Bogacik, "Status of LEU Programs at Babcock & Wilcox," *Reduced Enrichment for Research and Test Reactors--Proceedings of an International Meeting, Petten, The Netherlands, October 14-16, 1985*, P. von der Hardt and A. Travelli, Eds., D. Reidel Publishing Company, Dordrecht, pp. 165-173 (1986).

16. S. Nazaré, "Low Enrichment Dispersion Fuels for Research and Test Reactors," J. of Nucl. Materials 124, 14-24 (1984).

17. P. Toft and A. Jensen, "Differential Thermal Analysis and Metallographic Examinations of U_3Si_2 Powder and U_3Si_2/Al (38 w/o) Miniplates," *Reduced Enrichment for Research and Test Reactors--Proceedings of an International Meeting, Petten, The Netherlands, October 14-16, 1985*, P. von der Hardt and A. Travelli, Eds., D. Reidel Publishing Company, Dordrecht, pp. 373-381 (1986).

18. T. C. Wiencek, "A Study of the Effect of Fabrication Variables on the Quality of Fuel Plates," Proc. 1986 Int. Mtg. on Reduced Enrichment for Research and Test Reactors, Gatlinburg, Tennessee, November 3-6, 1986, Argonne National Laboratory Report ANL/RERTR/TM-9, in press.

19. *CRC Handbook of Chemistry and Physics*, 64th Edition, R. C. Weast, Ed., CRC Press, Boca Raton, pp. D-43 and D-44 (1983).

20. R. K. Williams, R. S. Graves, R. F. Domagala, and T. C. Wiencek, "Thermal Conductivities of U_3Si and U_3Si_2-Al Dispersion Fuels," Proc. 19th Int. Conf. on Thermal Conductivity, Cookeville, Tennessee, October 21-23, 198[illegible], in press.

21. R. R. Hobbins, EG&G Idaho, unpublished information (1973).

22. G. L. Copeland and M. M. Martin, "Development of High-Uranium-Loaded U_3O_8-Al Fuel Plates," Nucl. Tech. 56, 547 (1982).

23. T. C. Wiencek, R. F. Domagala, and H. R. Thresh, "Thermal Compatibility Studies of Unirradiated Uranium Silicide Dispersed in Aluminum," Nucl. Tech. 71, 608-616 (1985).

24. C. E. Weber, "Progress on Dispersion Elements," *Progress in Nuclear Energy*, Ser. V, 2, Pergamon Press, N.Y. (1959).

25. R. F. Domagala, T. C. Wiencek, J. L. Snelgrove, M. I. Homa, and R. R. Heinrich, "Differential Thermal Analysis of U_3Si-Al and U_3Si_2-Al Reactions," Argonne National Laboratory Report ANL/RERTR/TM-7 (October 1984) and Am. Cer. Soc. Bull. 65(8), 1164-70 (1986).

26. S. Nazaré, "Reaction Behavior of U_xSi_y- and U_6Fe-Al Dispersions," Proc. 1984 Int. Mtg. on Reduced Enrichment for Research and Test Reactors, Argonne, Illinois, October 15-18, 1984, Argonne National Laboratory Report ANL/RERTR/TM-6 (Conf-8410173), pp. 39-46 (July 1985).

27. A. E. Pasto, G. L. Copeland, and M. M. Martin, "Quantitative Differential Thermal Analysis Study of the U_3O_8-Al Thermite Reaction," Am. Cer. Soc. Bull., 61(4), 491-496 (1982).

28. J. D. Fleming and J. W. Johnson, "Aluminum-U_3O_8 Exothermic Reactions," Nucleonics, 21(5), 84-87 (May 1963).

29. R. L. Senn and M. M. Martin, "Irradiation Testing of Miniature Fuel Plates for the RERTR Program," Oak Ridge National Laboratory Report ORNL/TM-7761 (July 1981).

30. G. L. Copeland, R. W. Hobbs, G. L. Hofman, and J. L. Snelgrove, "Performance of Low-Enriched U_3Si_2-Aluminum Dispersion Fuel Elements in the Oak Ridge Research Reactor," Argonne National Laboratory Report ANL/RERTR/TM-10 (October 1987).

31. C. Baas, M. Barnier, J. P. Beylot, P. Martel, and F. Merchie, "Progress Report on LEU Fuel Testing in CEA Reactors," Proc. 1986 Int. Mtg. on Reduced Enrichment for Research and Test Reactors, Gatlinburg, Tennessee, November 3-6, 1986, Argonne National Laboratory Report ANL/RERTR/TM-9, in press.

32. F. Merchie, CEN-G, personal communication (July 1987).

33. J. M. Beeston, R. R. Hobbins, G. W. Gibson, and W. C. Francis, "Development and Irradiation Performance of Uranium Aluminide Fuels in Test Reactors," Nucl. Tech. 49, 136-149 (June 1980).

34. G. L. Hofman, G. L. Copeland, and J. E. Sanecki, "Microscopic Investigation into the Irradiation Behavior of U_3O_8-Al Dispersion Fuel," Nucl. Tech. 72, 338-344 (1986).

35. A. E. Richt, R. W. Knight, and G. M. Adamson, Jr., "Postirradiation Examination and Evaluation of the Performance of HFIR Fuel Elements," Oak Ridge National Laboratory Report ORNL-4714 (December 1968).

36. D. Stahl, "Fuels for Research and Test Reactors, Status Review: July 1982," Argonne National Laboratory Report ANL-83-5, pp. 37-39 (December 1982).

37. R. E. Woodley, "The Release of Fission Products from Irradiated SRP Fuels at Elevated Temperature," Hanford Engineering Development Laboratory Report HEDL-7598 (June 1986).

38. T. Shibata, T. Tamai, M. Hayashi, J. C. Posey, and J. L. Snelgrove, "Release of Fission Products from Irradiated Aluminide Fuel at High Temperatures," Nucl. Sci. and Eng. 87, 405-417 (1984).

39. J. C. Posey, "Release of Fission Products from Miniature Fuel Plates at Elevated Temperatures," Proc. Int. Mtg. on Research and Test Reactor Core Conversions from HEU to LEU Fuels, Argonne, Illinois, November 8-10, 1982, Argonne National Laboratory Report ANL/RERTR/TM-4 (CONF-821155), pp. 117-133 (September 1983).

40. G. W. Parker, G. E. Creek, C. J. Barton, W. J. Martin, and R. A. Lorenz, "Out-of-Pile Studies of Fission-Product Release from Overheated Reactor Fuels at ORNL, 1955-1965," Oak Ridge National Laboratory Report ORNL-3981 (July 1967).

41. G. C. Rodrigues and A. P. Gouge, "Reprocessing RERTR Silicide Fuels," Savannah River Laboratory Report DP-1657 (May 1983).

42. U.S. Department of Energy, "Receipt and Financial Settlement Provisions for Nuclear Research Reactor Fuels," Federal Register 51(32), 5754-5756 (February 18, 1986) and Federal Register 51(42), 7487 (March 4, 1986).

DISTRIBUTION FOR ANL/RERTR/TM-11

Internal:

A. Schriesheim
C. E. Till
P. I. Amundson
L. Burris
D. W. Cissel
L. G. LeSage
R. A. Lewis
J. F. Marchaterre
R. J. Teunis
D. C. Wade
R. W. Weeks
A. Travelli (150)
J. L. Snelgrove (2)
R. F. Domagala (2)
G. L. Hofman (2)
F. J. Karasek
L. A. Neimark
D. R. Schmitt
H. R. Thresh
T. C. Wiencek (2)
ANL Contract File
ANL Patent Department
ANL Libraries (3)
TIS Files (6)

External:

DOE-TIC, for distribution per UC-83 (41)

Manager, Chicago Operations Office, DOE

Director, Technology Management Div., DOE-CH

J. P. Colton, ACDA
D. E. Bailey, DOE-NE
L. S. Rubenstein, NRC (2)
D. Stahl, SAI

ORNL:

E. D. Clemmer
G. L. Copeland (2)
R. W. Hobbs (2)
S. S. Hurt
R. W. Knight
D. L. Selby
R. L. Senn (2)
L. G. Shrader
J. H. Swanks
C. D. West

INEL:

K. R. Brown
R. E. Carter
C. H. Cooper
R. R. Hobbins
J. A. Lake
L. K. Seymour

C. Benjamin Alcock, The University of Toronto
Paul C. Shewmon, Ohio State University

Applied Physics Division Review Committee:

Paul W. Dickson, Jr., EG&G Idaho, Inc.
E. Linn Draper, Gulf State Utilities
Michael J. Driscoll, Massachusetts Institute of Technology
Robert L. Hellens, West Simsbury, Connecticut
William E. Kastenberg, University of California-L.A.
Daniel A. Meneley, University of New Brunswick
Warren F. Miller, Los Alamos National Laboratory

Changed Pages of ANL/RERTR/TM-10

List of Figures (Cont.)

List of Figures (Cont.)

Table I. Materials Used in U_3Si_2 Test Elements

Part Name	Fabricators		
	B&W	CERCA	NUKEM
Fuel Plate			
Frame	6061	AG 3 NE	AlMg2
Cover	6061	AG 3 NE	AlMg2
Fuel Core			
Fuel	U_3Si_2	U_3Si_2	U_3Si_2
Matrix	MD X75	A5 NE or AL 405	Al-Powder 99.8
Side Plate	6061-T6	AG 3 NE	AlMgSi1, F32
Comb	6061-T6	6061-T6[a]	AlMgSi1, F32
Pin (Rivet)	4043 or 5356	4043 or 5356[a]	AlMgSi1, F21
End Adapter	356 Al	356 Al[a]	356 Al[a]
Welding Wire	N/A	AG 3 NE	S-AlSi5

[a]Supplied by ORNL/ANL.

Table II. Properties of Aluminum Alloys Specified for ORR LEU Fuel Elements

Alloy[a]	AlMg2	AG 3 NE	6061	6061-T6	AlMGSi1, F32
Composition, wt%[b]					
Al[c]	97.6	96.7	97.6	97.6	97.2
Mg	2.0	2.7	1.0	1.0	0.9
Si	<0.3	<0.3	0.6	0.6	1.0
Cu	<0.05	<0.008	0.28	0.28	<0.05
Cr	<0.3	<0.3	0.2	0.2	<0.25
Mn	<0.05	<0.7	<0.15	<0.15	0.7
Tensile Strength, MPa	>147	235	124	310	>314
Yield Strength, MPa	>59	127	55	276	>255
Hardness (HB)	40	42	30	95	95
Thermal Conductivity, W/m·K	150	130	180	167	170
Heat Capacity, J/kg·K	---	960	896	896	---
Solidus Temperature, °C	620	---	582	582	585
Liquidus Temperature, °C	650	650	652	652	650

[a]All properties are for O-temper anneal unless listed otherwise.
[b]Average value of composition limit range used.
[c]Typical Al contents are provided for comparison purposes only. The specification is for Al to constitute the remainder after accounting for additions and impurities.

the inner and outer plates, respectively. Surface defects with depths up to 0.127 mm (0.005 in.) were allowed, leaving a minimum of 0.20 mm (0.008 in.) of cladding over the fuel meat at any point. With only 12 vol% of fuel in the fuel meat of the HEU plates, it was relatively easy to meet these requirements. At the 42-vol% fuel loading required for the LEU plates, however, the rolling process tends to leave the fuel meat thicker at the ends than in the middle (commonly referred to as a dogbone). This, of course, results in thinner cladding over the dogbones. In addition the large concentration of fuel particles results in an increased probability that several fuel particles will come into contact with each other and that one of them will be pushed into the cladding. Both of these phenomena would have resulted in a reduced yield of plates meeting the original ORR minimum cladding thickness specification. ORNL agreed to a minimum cladding thickness specification of 0.267 mm (0.0105 in.) for the inner fuel plates and 0.40 mm (0.016 in.) for the outer plates. They also agreed to allow a 0.25-mm (0.010-in.) minimum at up to six points in the sections to be examined from any one fuel plate. If the plates exhibited dogbones, the depth of surface defects was limited to 0.076 mm (0.003 in.) in the dogbone region in order to maintain approximately the same absolute minimum cladding thickness as for the HEU fuel plates.

Also related to the high volume loading of fuel in the meat is an increased number of fuel particles at the surface of the fuel compact and, consequently, an increased probability for fuel particles to become dislodged and spread into nominally fuel-free zones during the rolling process. This phenomenon, referred to as fuel flaking or fuel out of zone, is identified by the occurrence of white spots on an x-radiograph of the fuel plate. Although the specifications approved for the LEU elements did not specifically address this new problem, ORNL used realistic criteria in judging the acceptability of plates with fuel out of zone. Since the amount of fission energy liberated in these relatively isolated particles is so small as to preclude any cooling problem, the only concern is the isolation of fission products. In general, it was required that no particle be within 0.5 mm (0.020 in.) of the edges or ends of fuel plates.

Another consequence of the high volume loading of fuel particles in the fuel meat and of the high uranium loading in each fuel particle was a difficulty in achieving as homogeneous a uranium loading as was possible in the HEU fuel meat. In addition, it was necessary to accept the spot size normally associated with each fabricator's scanning equipment since it was impractical to request that special collimators be installed for such limited work under a cooperative arrangement. The homogeneity tolerances to which each fabricator agreed are shown in Table III. It is apparent that the different sets of requirements yield different degrees of homogeneity. All were acceptable to ORNL, however.

Finally, the HEU element specifications required a metallographic grain growth test to verify a metallurgical bond between covers (cladding) and frame. The fabricators were allowed to substitute a bending (delamination) test of a strip of material trimmed from the end of the plate. In addition, it was required that each fuel plate be ultrasonically scanned to detect the

Table III. Comparison of Homogeneity Tolerances for U_3Si_2 Test Elements

	Spot Size		Tolerance	
	Linear, mm	Area, mm^2	Dogbone Region	Non-Dogbone Region[a]
HEU Element	2.0 diam	3.1	+27%/-100%	+27%/-100%
	2.0 × 12.7	25.4	+12%/-100%	±12%
B&W LEU Element	2.0 diam	3.1	+30%/-100%	---
	20 × 2.0 diam[b]	62.8	---	±10%
CERCA LEU Element	3.0 diam	7.1	+27%/-100%	±27%
	5.0 diam	19.6	---	±12%
NUKEM LEU Element	5.6 diam	24.6	+27%/-100%	±12%

[a]In the area between the maximum and minimum core outlines a tolerance of -100% was used in place of the listed negative tolerance.
[b]Twenty spots distributed along a 25.4-mm (1.0-in.) line.

presence of non-bond areas in the fuel zone. It was recognized that false non-bond indications might occur from reflections at the fuel-frame interface, so the fabricators were given considerable latitude in interpreting the ultrasonic records in this region. Primary reliance was placed on the blister test to detect non-bonds at the fuel-frame interface.

2.3 As-Fabricated Attributes

The stoichiometric composition of U_3Si_2, 7.3 wt% Si, was chosen by each fabricator as the nominal composition of the fuel compound. Metallic uranium and silicon were combined by arc-melting to form the fuel alloy. Since it is a practical impossibility to produce a perfectly homogeneous ingot by arc melting, the as-cast ingots consisted of U_3Si_2 as the major phase with minor amounts of USi and uranium solid solution (U_{ss}, also called free uranium). Both CERCA and NUKEM heat treated the ingots for approximately three days at 800°C, as had been the practice at ANL for the U_3Si_2 used in the miniplates. During this heat treatment, most or all of the U_{ss} was converted to U_3Si through the peritectoid reaction. By the time B&W began production, however, it had been decided at ANL that no advantage was to be gained by heat treating U_3Si_2. Therefore, the B&W fuel was not heat treated. As will be discussed later, a knowledge of the differences in the compositions of the fuel powders used in the elements from the different fabricators was important in understanding the details of the irradiation behavior of the different elements.

The results of chemical and spectroscopic analyses of the fuel powders produced by the three fabricators are given in Table IV. The maximum U_3Si_2 particle size was 150 μm for B&W and NUKEM and 90 μm for CERCA. The quantity of fines (particles smaller than 40 μm for CERCA and NUKEM or 44 μm for B&W) in the powder was 17% for NUKEM, 18% for B&W, and 40% for CERCA.

The minimum cladding thickness specification was discussed in Section 2.2. Smaller values of this parameter were discovered during metallographic examination of plates during fabrication. The following minima were accepted: 0.22 mm (0.0087 in.) for B&W, 0.23 mm (0.0091 in.) for NUKEM, and 0.25 mm (0.0098 in.) for CERCA. One must understand, of course, that the penetration of fuel particles into the cladding is a random process and that the actual minima for the fuel plates assembled into elements are not necessarily the same as those measured in the sections of the plates destructively examined.

Another parameter of importance in understanding the swelling characteristics of the fuel plates is the volume of void in the as-fabricated fuel plates. Void volumes were measured by the fabricators and/or by ANL using the immersion density technique. The results for inner plates were 4.0 vol% for CERCA and 6.8 vol% for NUKEM. The results for outer plates were 7.8 vol% for NUKEM and 9.9 vol% for B&W.

The immersion density measurements mentioned above yield the fuel meat volume of each plate measured. Based upon these measurements, the calculated

Table IV. Reported Average U_3Si_2 Powder Compositions and Impurities

Major Constituent, wt%	Fabricator		
	B&W	CERCA	NUKEM
U	91.8 (91.2-92.3)	92.1	---
Si	7.4 (7.2- 7.7)	---	7.3
Impurity, ppm			
Al	4	---	400
B	5	<10	0.9
C	607	337	400
Cd	<0.5	<10	<5
Co	---	---	<5
Cu	7	---	96
Fe	6	---	550
H	---	13	---
Li	---	<5	<5
N	---	1672	---
Ni	5	---	---
O	806	1290	---
Zn	<2	---	<10

average uranium densities for the fuel plates from each fabricator are 5.2 Mg U/m^3 for the CERCA elements, 4.9 Mg U/m^3 for the NUKEM elements, and 4.6 Mg U/m^3 for the B&W elements, compared to the 4.75 Mg U/m^3 nominal uranium density. The as-fabricated uranium densities correspond to fuel volume fractions of 46, 43, and 41 vol% for the CERCA, NUKEM, and B&W fuel, respectively. These density data are consistent with average fuel meat thicknesses determined from metallographic studies by CERCA and B&W--0.49 mm and 0.53 mm, respectively.

3. IRRADIATION HISTORY

The irradiation history of the U_3Si_2 test elements is summarized in Table V. One element of each pair was irradiated to approximately normal (~50% average) burnup in the ORR. The second element was irradiated until more than 75% average burnup was achieved. Element No. NSI-201, one of the first pair of elements to be irradiated, was removed from the core earlier than planned in order to take advantage of two months of cooling during a major maintenance outage so that the postirradiation examination of the element would not be delayed.

The two basic core configurations employed during the irradiation of the U_3Si_2 test elements are shown in Fig. 2. At various times, experiments were replaced with filler pieces or with fuel elements. Although the test elements were not cycled through the core in a normal pattern, they did experience irradiation in a variety of typical core positions.

Although fluxes were measured for only a few of the cores containing these elements, results of calculations of similar cores have been used to estimate the maximum powers and associated heat fluxes and temperatures of the test elements during irradiation. It is estimated that each element produced ~1.3 MW during its first cycle of irradiation, with a peak-to-average power density and heat flux factor of no more than 1.5. The average heat transfer area of the element is 1.39 m^2, giving average and peak heat fluxes of 0.94 and 1.4 MW/m^2, respectively. Estimated temperature drops from the center of the fuel meat to the bulk coolant are given in Table VI for various materials and assumptions. The maximum temperature drops given in the table are overestimates since it took several cycles for the boehmite film to build up to its maximum thickness, by which time the element power had decreased owing to burnup. With an average bulk coolant temperature in the ORR core of ~53°C, it is estimated that peak fuel meat temperatures were between 110 and 130°C during the early cycles of irradiation. Average fuel meat temperatures are estimated to have been ~20 to 25°C less.

The pH and electrical resistivity of the primary coolant during the irradiation of the elements ranged between 5.0 and 6.3 and 0.7×10^4 and 2.5×10^4 Ω·m, respectively.

Table V. Irradiation History Summary for U_3Si_2 Test Elements

Core Position	Irradiation Time, fpd					
	BSI-201	BSI-202	CSI-201	CSI-202	NSI-201	NSI-202
B-3	24.8		25.7	43.1		12.6
B-7		24.8	43.1	25.7		
C-2	27.1	12.5	42.7	9.4		
C-4		174.9	12.6	54.9		29.0
C-5		24.9				70.3
C-6	24.9			112.0		54.9
C-8	12.5	27.1	9.4	42.7		
D-2		12.7			57.0	60.8
D-3		30.0				
D-7	30.0					
D-8	12.7				53.2	57.0
E-2				11.5		
E-8			11.5			
Total	132.0	306.9	145.0	299.3	110.2	284.6
Begin Irrad.	11/23/83	11/23/83	4/28/83	4/28/83	5/27/82	5/27/82
End Irrad.	4/22/84	12/19/84	9/29/83	8/14/84	1/14/83	8/14/84
Total No. of Cycles	8	26	11	26	8	24
Ave. Burnup,[a] % 235U	54	77	52	82	35	82
Ave. Burnup,[b] MWd	150	217	144	228	95	231
Ave. Power, MW	1.13	0.71	0.99	0.76	0.86	0.81

[a] See Table VIII.

[b] Based on the following calculated ^{235}U burnup rate correlation:

Burnup rate (g/MWd) = 1.2608 - 0.0004103 · Burnup (MWd).

Table VI. Estimated Average and Peak Fuel Temperature Drops

	Thickness, mm	Thermal Conductivity, W/m·K
Fuel Meat	0.25[a]	30 - 60[b]
Cladding	0.38	130 - 180[c]
Boehmite Layer	0 - 0.025	2.25

	Temperature Drops, °C	
	Average (0.94 MW/m^2)	Peak (1.4 MW/m^2)
Fuel Meat		
30 W/m·K	7.8	11.7
60 W/m·K	15.7	23.3
Cladding		
130 W/m·K	2.7	4.1
180 W/m·K	3.8	5.7
Boehmite		
13 μm thick	5.4	8.1
25 μm thick	10.4	15.6
Water Film[d]	27.6	41.2
Total		
Minimum (no Boehmite)	38.1	57.0
Maximum	57.5	85.8

[a] Half-thickness.

[b] R. K. Williams, R. S. Graves, R. F. Domagala, and T. C. Wiencek, "Thermal Conductivities of U_3Si and U_3Si-Al Dispersion Fuels," Proc. 19th International Conference on Thermal Conductivity, Cookeville, Tennessee, USA, October 21-23, 1985, in press.

[c] See Table II.

[d] Film coefficient calculated using the Dittus-Boelter correlation for a bulk water temperature of 53.3°C.

The accessible channel gaps of the elements were measured at various times during the irradiation of the elements (following each cycle beyond 50% burnup) using the ultrasonic probe described in Ref. 3. In all cases the channel profiles remained essentially unchanged during the course of the irradiations, indicating no abnormal swelling or warping of the plates.

4. POSTIRRADIATION EXAMINATION OF FUEL ELEMENTS

After suitable periods of cooling in the ORR pool following completion of irradiation, the elements were transported to the ORNL High-Radiation-Level Examination Laboratory (HRLEL). All six elements were given the complete nondestructive and destructive examinations outlined in Appendix A. The nondestructive portion consisted of visual examination, dimensional inspection, gamma scanning, and coolant channel measurements. Then, the elements were dismantled, and the plates were visually inspected. Selected plates were measured for thickness and were gamma scanned. Two plates from each element were tested for blister threshold temperature, and one plate from each element was sectioned for microstructural and burnup analyses.

4.1 Visual Examination

The elements were examined visually through the cell windows and through the Kollmorgan periscope. All six of the elements appeared to be in excellent condition. With the exception of the oxide film and some handling scratches, the elements appeared to be as fabricated. No abnormal conditions were observed. Photographs obtained of the exterior of the elements and through the coolant channels are contained in Appendix B.

4.2 Dimensional Inspection

The width (between side plate outer surfaces) and stack height (between outer fuel plate outer surfaces) of each element were measured at six axial locations along a central line and along parallel lines near the edges of the element. The measurements were made by positioning the element between opposing dial micrometers at the desired point of measurement and comparing the readings to a standard. By comparing readings from the upper and lower micrometers, bow or twist could be detected. The length of each element was determined by comparison to a standard using a fixture and a dial indicator. No unusual bow, twist, or swelling was observed for any of the elements. Within the accuracy of the in-cell measurements, the dimensions were within the envelope of tolerances allowed for as-fabricated dimensions. A summary of the dimensional measurement result is given in Table VII. Individual measurement results for each element are presented in Appendix C.

Table VII. Results of Dimensional Inspection of Irradiated Elements

	Width,		Stack Height,		Length,	
	mm	in.	mm	in.	mm	in.
Fabrication Tolerance						
Max	76.10	2.996	78.18	3.078	975.1	38.390
Min	75.84	2.986	77.67	3.058	973.5	38.328
Element No.						
BSI-201	76.17	2.999	77.83	3.064	975.0	38.386
	75.72	2.981	78.31	3.083		
BSI-202	76.20	3.000	77.85	3.065	974.8	38.378
	76.05	2.994	77.75	3.061		
CSI-201	76.07	2.995	78.05	3.073	---	---
	75.82	2.985	77.09	3.035		
CSI-202	75.69	2.980	78.10	3.075	974.5	38.367
	75.56	2.975	77.50	3.051		
NSI-201	75.95	2.990	78.10	3.075	974.5	38.365
	75.84	2.986	77.93	3.068		
NSI-202	76.23	3.001	78.26	3.081	975.7	38.413
	76.02	2.993	78.00	3.071		

4.3 Gamma Scanning of Elements

The elements were passed in front of a 432-mm (17-in.)-long collimator with a 0.25 mm × 25.4 mm (0.010 in. × 1.0 in.) aperture, and the gamma spectrum was measured. The detector was either a NaI or a Ge(Li) crystal. During the course of the work, several methods of recording the data were used. Profiles of gamma intensity versus axial position were obtained for integrated energies greater than 0.5 MeV and for a narrow energy window containing the ^{137}Cs peak at 662 keV. At certain positions, complete multichannel energy spectra were obtained using the Ge(Li) crystal.

The primary purpose of these measurements was, in conjunction with the results of the destructive burnup analyses discussed in Section 5.3, to provide data for determining burnups of similar elements not scheduled to be destructively examined. Since all of the present elements were destructively examined, including burnup analysis, these data will not be discussed in detail. The ^{137}Cs profiles are presented in Appendix D.

4.4 Coolant Channel Gap Thickness Measurements

Following removal of the end adapters from the elements, the coolant channel gap thicknesses were measured on either side of the comb along the entire length of each channel. For element NSI-201 the measuring probe was a spring-loaded device containing a linear voltage differential transformer (LVDT). Channel gaps of elements CSI-202, BSI-201, and BSI-202 were measured using a capacitance probe. For elements NSI-202 and CSI-201 neither device was available, and a 2.64-mm (0.104-in.)-diameter wire was rolled between the plates to assure that the channels exceeded the 2.64-mm minimum gap allowed by the specifications.

Tabulated results of the coolant channel measurements are contained in Appendix E. These data indicate that the gaps of all but a few channels everywhere exceeded the as-fabricated minimum dimension. In these few channels, the gap thicknesses at a few isolated points were slightly below this value (but greater than 2.62 mm). No comparable preirradiation data are available to determine changes. The uniformity of the channels indicates that no excessive swelling or warping of the plates occurred during irradiation.

5. EXAMINATION OF FUEL PLATES

The individual plates were removed from the element by cutting through the side plates into the coolant channels using a milling machine. The strips of aluminum clinging to the plate were then easily pulled off without damaging the plate.

5.1 Visual Inspection of Plates

The first examination of the plates following their removal from the element was verification of the plate numbers and a thorough visual inspection. The plates in all elements exhibited some warping and bowing after removal from the element. This is typical of all irradiated elements of this configuration. All of the plates from the six elements appeared to be in good condition with no evidence of blisters, excessive swelling, or any other unusual condition.

5.2 Plate Thickness Measurements

Plate thickness measurements were made by positioning the plate between opposing dial micrometers at the desired point of measurement and comparing the readings to a standard. The indicator tip for the top (convex) surface was a 6.35-mm (1/4-in.)-diam flat and for the bottom (concave) surface was a 3.18-mm (1/8-in.)-diam ball. Measurements were made along tracks at the center and near the sides of the plate. No attempt was made to remove the oxide film from the plates, so its thickness is included in the overall plate thickness. Near the end of the examinations, a new device based on capacitance became available to measure the plate thickness. This device was used to remeasure the thickness of several plates as an overcheck of the micrometer measurements and to supplement some incomplete data. Thicknesses determined with the new device were consistent with the data obtained using the micrometers.

All plates of NSI-201 and NSI-202 were measured at NUKEM's request, since they were the first U_3Si_2 elements to be irradiated. Five plates (in positions 2, 6, 10, 14, and 18) from each of the other four elements were selected for measurement. Plate thickness increases were determined from the thicknesses measured at each position by subtracting the plate thickness measured outside the fuel zone, near the end of the plate. This method at least partially corrects for the oxide film buildup, since the normalization region also has an oxide film, though probably not as thick a one as in the fuel zone, where the heat flux was higher. The average fuel plate thickness increases in the peak- and minimum-burnup regions (based upon the plates in positions 2, 6, 10, 14, and 18) are listed in Table VIII. Swelling profiles for the five plates used for the averages are presented in Appendix F.

Apart from the contribution from the oxide film, plate thickness changes result only from swelling of the fuel meat. Since the fuel meat is well constrained by the frame in the transverse directions, it swells almost exclusively in the thickness direction. The fractional change in fuel meat thickness is, then, equal to the fractional change in fuel meat volume, the number most commonly reported as the fuel meat swelling. Experience with well over 100 miniplates, where both fuel plate thickness changes and fuel meat volume changes were accurately measured, has shown that swelling estimates based on thickness changes are always greater than the actual fuel meat volume changes since the thicknesses are measured between the "high" points on the

Table VIII. Average Thickness Increase and Burnup[a]

Element No.	Low-Burnup End			Peak-Burnup Region			Element-Average Burnup, %
	Burnup, %	Thickness Increase, mils	μm	Burnup, %	Thickness Increase, mils	μm	
BSI-201	28	0	0	69	1.5	38	54
BSI-202	53	0	0	97	1.8	46	77
CSI-201	32	0.1	3	66	1.7	43	52
CSI-202	55[b]	0.9	23	98	4.4	112	82
NSI-201	19	0.7	18	46	1.0	25	35
NSI-202	53	1.2	30	97	4.1	104	82

[a]Average thickness increases and burnups at the low-burnup end and in the peak-burnup region are average values for the plates in positions 2, 6, 10, 14, and 18. Data from all 19 plates were used in calculating the element-average burnup.

[b]Based on analyzed burnup and comparison to other elements because of discrepant data at the low-burnup end.

fuel plate surfaces. The curvature of the ORR fuel plates increases this problem. Therefore, no attempt has been made to calculate volume swelling from the thickness change data. Nevertheless, significant differences in measured thickness change do represent significant differences in the volume swelling of the fuel meat. However, from the point of view of fuel element performance, the overall thickness changes were small compared to the allowed tolerance in the channel gap thickness. This is consistent with the results from the channel gap thickness measurements discussed in Sections 3 and 4.4.

5.3 Plate Gamma Scanning and Burnup Analysis

Five plates from each element (including the one from which burnup samples were taken) were selected for determining the axial burnup profile by gamma scanning. The setup and techniques described in Section 4.3 for full-element scanning were also used for the plates. Complete multichannel energy spectra were obtained with the Ge(Li) crystal at the peak-burnup points of all nineteen plates of each element, with the exception of NSI-201.

Samples for burnup analysis were obtained at the positions of peak and minimum burnup, as determined by the gamma profiles. Following dissolution of the sample, the relative uranium and plutonium isotopic abundances were determined by mass spectrometry. The ^{235}U isotopic abundances before and after irradiation were used, with calculated correlations for changes in the ^{238}U and ^{236}U abundances, to derive the ^{235}U burnup.

Relative plate-average burnups were determined from the individual axial profiles, and the relative plate-to-plate burnup profile in the element was determined from the areas of the 662 keV peak of ^{137}Cs in the multichannel spectra (NaI gamma intensity data used for NSI-201) at the peak-burnup point of each plate. These data were normalized to the results of the destructive burnup analysis to determine the element-average burnup. The results are summarized in Table VIII. Typical profiles are shown in Fig. 3. Typical examples of the gamma scanning data and the complete burnup analysis data and correlations are in Appendix G.

As was mentioned in Section 3, the average burnup of one element from each fabricator was intentionally pushed well beyond the ~50% level normally achieved in reactors using this type of fuel. This resulted in peak burnups of ~98% in each case. Accounting for non-^{235}U fissions, the fission density in the high-burnup elements ranged between $\sim 1.1 \times 10^{27}$ and $\sim 2.5 \times 10^{27}$ f/m^3.

5.4 Blister Threshold Testing

A method which has been used historically to compare the relative irradiation performance of dispersion plate-type research reactor fuels is their resistance to blistering during heating after irradiation. This test, termed the "blister threshold test," is performed by sequentially heating the plate (or portions thereof) to higher and higher temperatures and visually examining the plate after each heating for evidence of blisters. Two plates from each

element were blister threshold tested. The entire plate rather than a plate section was heated to preclude the possibility of fission gas diffusing out of the cut edges rather than causing blisters at these relatively high volume fractions of fuel. The plates were held at the following temperatures for 30 minutes; removed from the furnace, cooled and examined; then heated to the next higher temperature (or removed from testing if blistering was observed): 400, 450, 475, 500, 525, 550, and 575°C. This procedure corresponds closely to the test procedure used previously for the highly enriched, low-volume-fraction uranium aluminide and uranium oxide fuels.

Typical blister threshold temperatures for the highly enriched dispersion fuels in use today range from 480 to >565°C for the uranium aluminide[7] and from 400 to >550°C for the uranium oxide[8] fuels. Blister threshold temperatures measured during miniplate tests of high-density, low-enriched uranium aluminide and uranium oxide dispersion fuels developed by the RERTR Program ranged from 550 to >550°C and from 450 to >550°C, respectively.[9] The same type of tests on uranium silicide miniplates yielded blister threshold temperatures of 530°C for U_3Si_2 fuel and 500 to 525°C for U_3Si fuel.[9]

The results of the present tests are presented in Table IX. The blister threshold temperature in each case was in the upper range of that which could have been expected with the established fuels. The appearance of the blisters was similar to that of the small blisters between the cladding and meat which were observed during testing of uranium silicide miniplates. The blister threshold temperatures of these full-sized plates are consistent with the results of the miniplate tests cited above. Photographs of the plates after blistering are contained in Appendix H.

These tests have shown that blister threshold temperatures of low-enriched, high-density uranium silicide fuels are about the same or higher than those of the highly enriched, lower-density uranium aluminide and uranium oxide fuels they are proposed to replace. Therefore, the propensity for blistering in-reactor will be no worse for these new fuels than for those presently in use.

5.5 Toughness of Irradiated Fuel Plates

Owing to the very high volume fraction of fuel particles in the meat following irradiation, some concern was expressed about the brittleness of the fuel and whether the fuel plates might be subject to breaking during handling and shipping. Even though one would expect the cladding and frame, which were fabricated from the same alloys used for HEU fuel plates for many years with no problems, and not the fuel meat to be the major determinant of the toughness of the fuel plate, it was considered prudent to devise a simple test to address this concern in a very qualitative manner.

Therefore, several high-burnup plates were bent to determine their ductility and toughness. The center of a plate was positioned under a mandrel

Table IX. Results of Blister Anneals of Full-Sized Plates

Element No.	Plate Position	Plate No.	Maximum Temperature, °C	Description of Blisters[a]
BSI-201	3	S-3-211-13	575	None
	8	S-3-210-23	575	Typical PI
BSI-202	3	S-3-213-15	550	Typical PI
	8	S-3-212-19	550	Typical PI
CSI-201	4	OSIIW-065	550	Typical PI
	8	OSIIW-054	550	Typical PI
CSI-202	3	OSIIW-044	550	Typical PI[b]
	8	CSIIW-026	550	Typical PI[c]
NSI-201	2	ORR-092	550	None
	8	ORR-100	550	None
	19	ORR-144	550	None
NSI-202	3	ORR-114	550	Typical PI
	9	ORR-123	550	Typical PI

[a]Typical PI--typical of postirradiation blisters observed previously in low-volume-fraction fuels (i.e., appear to be discrete blisters between meat and cladding with no "pillowing").
[b]Small blisters off of fuel formed at 500°C.
[c]Small blisters off of fuel formed at 525°C.

(~2.5 mm diam), and, with one end fixed, the plate was bent around the mandrel with the concave surface inward. A plate from CSI-202 broke at about 160° of bend. One plate from BSI-202 broke at about 90° of bend. Another plate from BSI-202 was bent 80° and straightened out completely when the force was removed. A plate from BSI-201, which had experienced significantly less neutron fluence, was bent 80° and straightened out when the force was removed. The same plate was the bent again to 90° and recovered to a bend of about 10° when the force was removed. The bent plates are shown in Fig. 4.

Therefore, it can be concluded that U_3Si_2 fuel plates in irradiated elements have more than adequate toughness to maintain their integrity during handling and shipping. The differences in the characteristics of the B&W and CERCA fuel plates demonstrated by the bending test are believed to be related primarily to differences in the cladding.

5.6 Metallography

The outermost of the inner plates on the concave side of each element was sectioned for destructive examination according to the diagram in Fig. 5. The burnup analysis sections were cut from the minimum- and maximum-burnup areas of the plate as determined by the gamma scan profile. Sections were cut immedi-ately adjacent to the burnup analysis sections for optical metallography, Scanning Electron Microscopy (SEM), and Scanning Auger Microscopy (SAM). In order to characterize the unirradiated fuel, a section from one plate produced by each fabricator during the fabrication run for the test elements was also examined.

The metallographic sections were prepared for viewing (transverse to the length direction of the plate) using conventional techniques. The section was mounted in epoxy, ground on progressively finer silicon carbide paper through 600 grit, then vibratorily polished. The vibratory polishing was a three step process. The first and second steps were on a Texmet* cloth with a water medium and 3-μm and 1-μm diamond paste respectively. The final polish was on Microcloth* with a thick water slurry of Magomet* for 12 minutes.

The SEM and SAM samples were small discs, approximately 1.5 mm in diameter, punched from the irradiated plates. These discs were split parallel to the cladding surface, yielding two samples of a fracture surface through the fuel meat. The small sample size was needed to reduce gamma activity enough to allow examination outside the hot cell. SEM and SAM examinations of the unirradiated plates were performed on polished metallography samples

Before proceeding with a discussion of the results of the metallographic examinations, some data obtained from miniplate irradiations that preceded the present full-sized fuel element experiments will be briefly reviewed. An example of the meat microstructure of a U_3Si_2 miniplate after >90% burnup is

*Texmet, Microcloth, and Magomet are trademarks of Buehler, Ltd.

shown in Fig. 6M.* Some of the noteworthy features in this optical micrograph are the absence of fission gas bubbles and the fact that all of the as-fabricated porosity has been consumed by fuel particle swelling. Fuel-aluminum interaction was limited to a narrow zone around the U_3Si_2 particles with a thickness about equal to the range of fission product recoils in aluminum. SEM examination of fractured fuel particles reveals a gas bubble morphology typical of pure U_3Si_2, as shown in Fig. 7M. The very uniform distribution of small gas bubbles that show no tendency to interlink is the reason for the stable swelling behavior of U_3Si_2.

The microstructural changes in U_3Si miniplates resulting from irradiation to high burnups are quite different, as shown in Fig. 8M. Fission gas bubbles are clearly visible in the optical micrograph. The bubble morphology, more clearly shown in the SEM images in Fig. 9M, reveals a basic difference in fission gas behavior between U_3Si and U_3Si_2. The fission gas bubbles in U_3Si are clearly not uniformly distributed and vary widely in size. The large bubbles are growing rapidly and linking up, resulting in a much larger fuel swelling rate than that of U_3Si_2. As will be shown further on in this report, the fuel in the full-sized U_3Si_2 plates exhibits characteristics of both U_3Si_2 and U_3Si.

Several uranium silicide miniplates fabricated with depleted uranium were irradiated to determine the effects of neutrons, as opposed to fission fragments, on the fuel. Figs. 10M and 11M clearly show that irradiation-enhanced diffusion has occurred.

The microstructure of the fuel as it changes during irradiation is discussed in alphabetical order for the three fabricators, beginning with the low-burnup plate in each case, followed by the high-burnup plate, and concluding with some observations on unirradiated fuel. The micrographs used in the discussion represent the typical fuel condition observed under the microscope. The serial number of the fuel element rather than that of the specific fuel plate from which the sample came is used for simplicity; plate numbers are the same as those from which burnup samples were taken (See Appendix G, Table G.8). Burnups are those measured for samples taken adjacent to the metallographic sections. Thickness changes are averaged for five plates from the element in order to reduce the considerable scatter in the data.

The B&W fuel meat microstructure at the low-burnup (31%) end of plate BSI-201 is shown in Figs. 12B-16B. A large fraction of the as-fabricated porosity is still present, and the fuel swelling that has taken place is easily accommodated by these pores. This is consistent with the fact that no

*A large number of photomicrographs are presented in this section, grouped by fabricator. So that each figure can easily be associated with the fabricator in the discussions to follow, a letter designating the fabricator has been appended to the remaining figure numbers, as follows: M - Miniplate (fabricated by ANL); B - B&W; C - CERCA; N - NUKEM.

thickness increase has occurred at this end of the plate. A narrow interaction zone between fuel particles and aluminum, as well as the rounding of the pores by radiation-enhanced diffusion, can be seen in Fig. 13B. Except for the somewhat-more-extensive Al-fuel interaction inside some of the particles, the structure is similar to that of irradiated depleted U_3Si_2 miniplates shown in Figs. 10M-11M. Figure 14B is a typical SEM image taken at the low-burnup end of the plate. The fuel appears free of fission gas bubbles at this magnification and the smoothed as-fabricated porosity is clearly evident. However, at higher magnification, areas containing small fission gas bubble populations were found in a few fuel particles, as shown in Figs. 15B and 16B. Figure 16B was taken using the backscatter electron (BSE) detector in order to show the different phases in the fuel more clearly. In this figure, as well as in the backscatter images to follow, the image intensity is proportional to the atomic number of the material. The light phase containing the small bubbles is, therefore, the highest U-Si phase present whereas the other extreme shading, black, represents matrix aluminum.

A considerably larger number of fission gas bubbles have formed in the fuel at the high-burnup (71%) end of plate BSI-201, and the fuel swelling has nearly consumed all as-fabricated porosity; only a few pores (the irregularly shaped ones in Figs. 17B and 18B) remain. Fuel swelling has resulted in a plate thickness increase of 38 μm at this location. The fuel has essentially three different phases with regards to gas bubble morphology: (1) the lighter phase that appears to be bubble free; (2) a light grey phase containing many very small bubbles; and (3) isolated irregular clusters of larger bubbles. SEM images, shown in Figs. 19B-22B, more clearly distinguish two very different bubble morphologies. The areas containing irregular, larger-sized bubbles look similar to U_3Si fuel observed in the miniplates, while areas containing dense and uniform small bubbles appear identical to U_3Si_2.

The low-burnup end of plate BSI-202 reached a burnup of 51%. No thickness increase was measured at the this location, and the fuel microstructure is not much different from that of the low-burnup end of plate BSI-201, as shown in Figs. 23B and 24B.

The high-burnup (97%) end of plate BSI-202 had a measured thickness increase of 46 μm, and, indeed, the fuel microstructure has somewhat-more-developed fission gas bubbles. As was the case at 71% burnup in plate BSI-201, three distinct phases exist in the fuel (see Figs. 25B-27B). The SEM images in Figs. 28B-33B show examples of the fission gas behavior in these three fuel phases. The major phase has a bubble morphology characteristic of pure U_3Si_2 (Fig. 33B), while parts of several fuel particles have either a characteristic U_3Si bubble morphology (Figs. 30B and 31B) or, as shown in Fig. 32B, a total absence of bubbles and apparent brittle properties reminiscent of UAl_4.

The different fission gas behavior in parts of the ostensibly pure U_3Si_2 fuel grains can be understood through the results of a detailed microscopic examination of an unirradiated fuel plate. As shown in Figs. 34B-36B, the

fuel particles are not single-phase U_3Si_2; rather, they contain both U_3Si and U, as determined by energy dispersive x-ray analysis (Fig. 37B). The Si-to-U ratios of phases A and B identify them as, respectively, U_3Si_2 and U_3Si, while the absence of Si in phase C indicates U_{ss}. Therefore, the U_3Si and U_3Si_2 show their characteristic irradiation behaviors, and the U_{ss} presumably reacts with Al during irradiation to form the stable UAl_4 compound. UAl_4 is indeed very stable and has never been found to contain fission gas bubbles. Therefore, the presence of U_{ss} in the as-fabricated fuel appears not to be detrimental to the performance of the fuel plate. This is consistent with the results of miniplate tests of UAl_2 fuel containing U_{ss} in the as-fabricated condition.[10] Even though the U_3Si was found to contain all the larger bubbles, its amount is such that no continuous network of large bubbles can develop, even at the very high burnup attained in these plates. It has been established in miniplate irradiations that interparticle linkup of larger bubbles is a prerequisite for possible large swelling in U_3Si.

The low-burnup (33%) end of plate CSI-201 may have just begun to show a thickness increase (3 μm was measured at this location). This may owe to the lower as-fabricated porosity of the CERCA plates (4%) than for the B&W plates (9 to 10%). Indeed the microstructure shown in Figs. 38C and 39C illustrates the rather low residual porosity at this burnup compared to that in the B&W plates discussed before (cf. Figs. 12B and 13B). The narrow interaction zone at the fuel particle surface is also seen in this fuel, but no significant amount of fuel-Al reaction phase inside the fuel particles is present.

The high-burnup (67%) end of plate CSI-201, with a thickness increase of 43 μm, has a fuel microstructure in which the fuel swelling has completely consumed the as-fabricated porosity and in which the fuel particles have begun to develop fission gas bubbles (see Figs. 40C and 41C). This is shown in more detail in the SEM images in Figs. 42C-45C. The phase in which larger bubbles occur (presumably U_3Si) is more dispersed, in a stringy or lacy manner, than in the B&W fuel.

The fuel microstructure at the low-burnup end (55%) of plate CSI-202 is very similar to that of plate CSI-201 (see Figs. 46C-51C). The thickness increase at this location is 23 μm.

The high-burnup (97%) end of plate CSI-202 has a measured thickness increase of 112 μm, more than twice that of the B&W plate. The fuel microstructure shows basically the same two-phase fission gas morphology seen in plate BSI-202, with the U_3Si-type bubbles more evenly distributed throughout the fuel (see Figs. 52C-57C). The total fission gas bubble volume appears to be significantly larger than that seen in the B&W plates, as would be expected from the much larger thickness increase experienced by the CERCA plates. Some of this larger thickness increase is attributable to the 4% porosity of the CERCA fuel meat compared to the 9-10% porosity of the B&W fuel meat, but the largest part of the difference undoubtedly owes to a larger amount of U_3Si in the CERCA plates.

The fission gas bubble behavior is, in fact, consistent with the as-fabricated fuel microstructure. The CERCA fuel did contain more U_3Si than did the B&W fuel (compare, for example, Figs. 58C and 34B), and it was more finely distributed than in the B&W fuel. The CERCA fuel did not contain U_{ss} because it had been heat treated, hence the absence of the UAl_4-like phase in the irradiated plate. It did, however, contain a powdery, grey phase (see Fig. 59C) which, by means of Auger Electron Spectroscopy, was found to contain oxygen and carbon in addition to U, Si, and Al. No trace of this material was found in the irradiated plates and it is assumed that it reacted in-pile to form a compound not distinguishable from the common fuel phases.

The fuel microstructure of the low-burnup (24%) end of NUKEM plate NSI-201 (shown in Figs. 61N-66N) was essentially the same as that of the low-burnup plates discussed before. The fuel consisted of U_3Si_2 with a somewhat coarsely distributed (compared to the CERCA fuel) second phase. The amount of second phase in this fuel appeared to be the highest of the three, albeit still minor. The second phase, and the tendency for gas bubbles to occur first in this phase, is more clearly illustrated in the microstructure at the high-burnup (51%) end of plate NSI-201, shown in Figs. 67N-72N. SAM analysis of the irradiated fuel positively identified the light phase containing the irregular bubbles in Fig. 72N as U_3Si, while the remainder of the fuel was identified as U_3Si_2.

The fuel at the low-burnup (54%) end of plate NSI-202, shown in Figs. 73N-78N, had the expected microstructure, with the beginning of small uniform bubble formation in U_3Si_2 (see Figs. 77N-78N) and continued irregular bubble development in U_3Si (see Fig. 76N). The high-burnup (96%) end of plate NSI-202, shown in Figs. 79N and 80N, had a measured thickness change of 104 μm. The fission gas bubble morphology is rather similar to that of the other high-burnup plates with a two-phase behavior, as clearly illustrated in Figs. 81N-83N.

As was the case for the B&W and CERCA fuels, the fission gas behavior can be traced to the microstructure of the as-fabricated fuel. The SEM images in Figs. 84N-87N show a major, dark grey, brittle phase, identified by energy dispersive x-ray analysis as U_3Si_2, interlaced with a more ductile light phase, U_3Si. The light phase occurs primarily in the largest fuel particles, acting as a bond during grinding, due to its more ductile properties. As indicated before, the NUKEM fuel appears to contain slightly more U_3Si than the CERCA fuel, and because this fuel was heat treated, it does not contain U_{ss}. It also does not contain the powdery oxy-carbide-like phase found in the CERCA fuel.

In conclusion, the metallographic observations are consistent with the relatively small plate thickness increases experienced during irradiation. The swelling is primarily caused by formation of two distinct fission gas bubble morphologies. The by-far-major phase, U_3Si_2, developed a very uniform and dense distribution of submicron-sized bubbles, characteristic of this

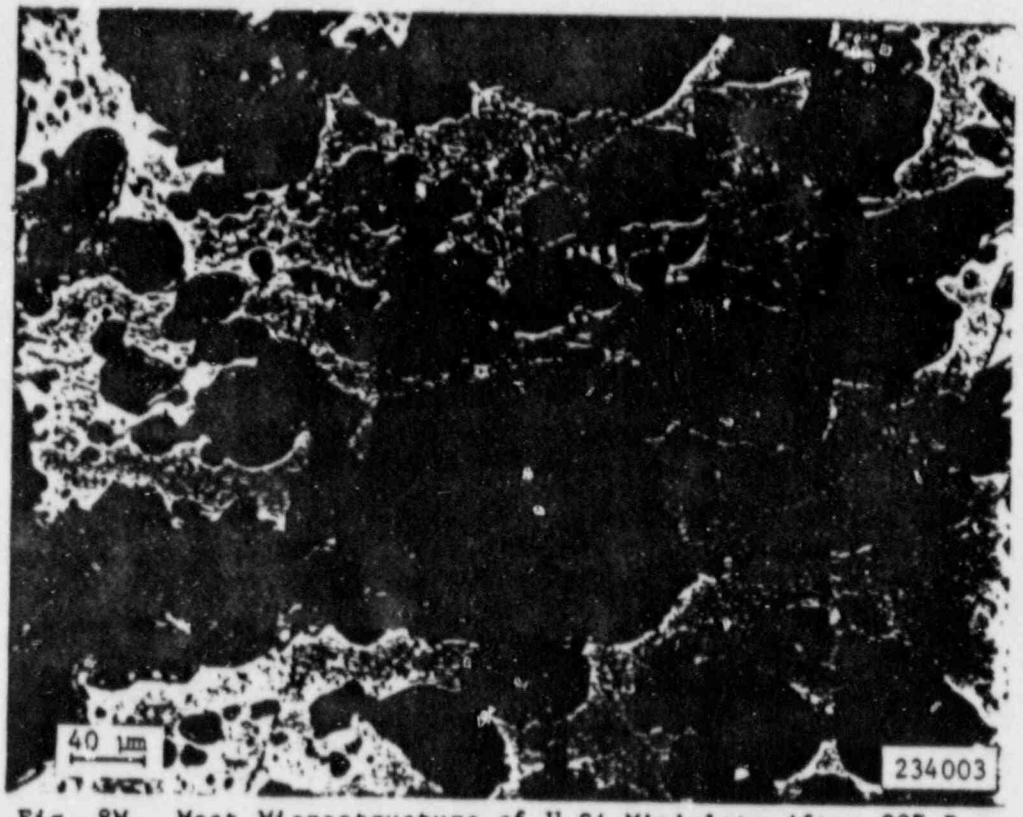

Fig. 8M. Meat Microstructure of U_3Si Miniplate After 90% Bu.

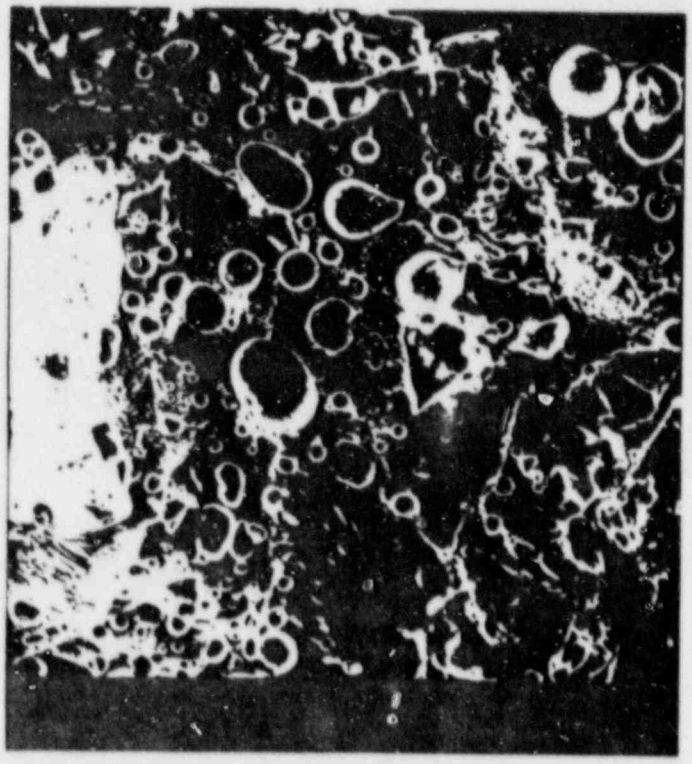

Fig. 9M. Fission Gas Bubble Morphology in U_3Si After 90% Bu.

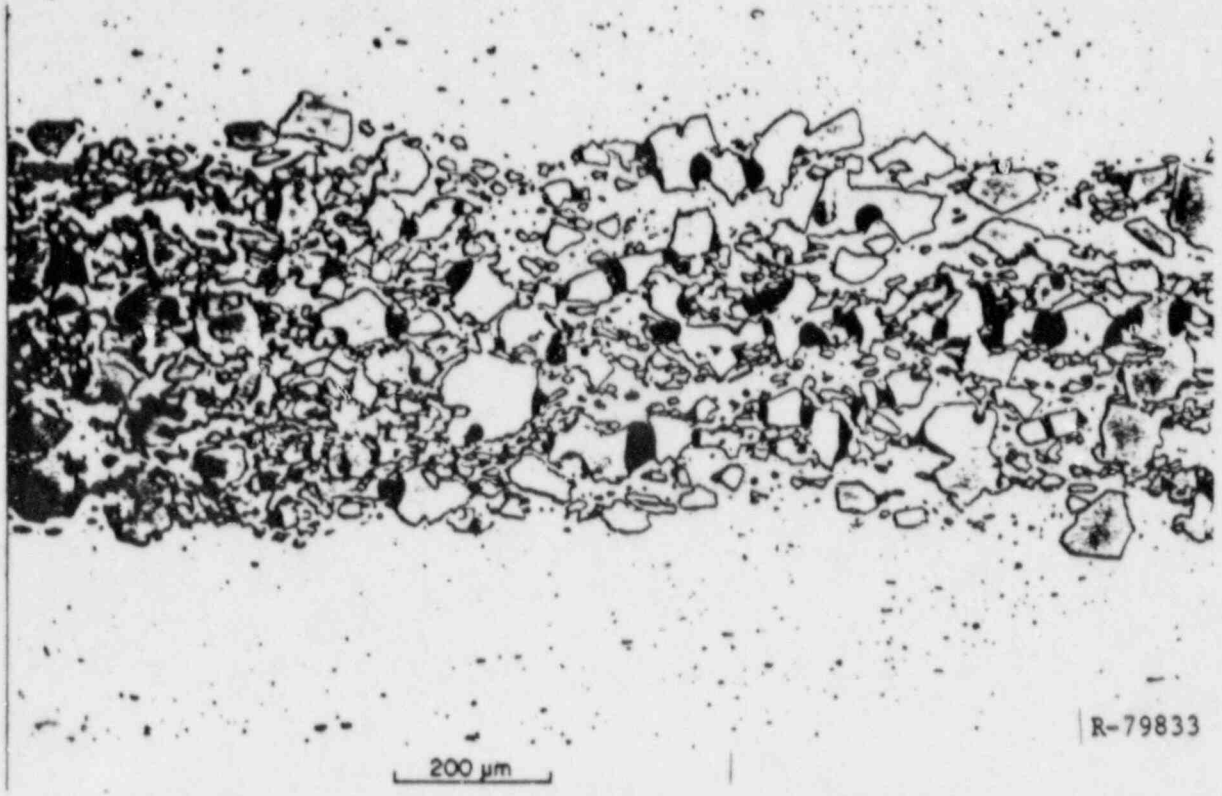

Fig. 10M. Meat Microstructure of Irradiated Depleted U_3Si_2 Miniplate.

Fig. 11M. Detail of Fig. 10M.

APPENDIX A

POSTIRRADIATION EXAMINATION STEPS

NONDESTRUCTIVE PIE

1. Visual Inspection

   Purpose: To observe general appearance and photograph.

   a. Observe general external appearance.
   b. Note any unusual features.
   c. Photograph element exterior with close-ups of unusual features.
   d. Photograph through channels with element backlighted.

2. External Dimensions

   Purpose: To determine dimensional changes during irradiation.

   a. Measure major external dimensions (length, width, depth).
   b. Determine amount of warp, twist, or bow.

3. Gamma Scanning of Full Element

   Purpose: To determine relative longitudinal burnup (fission product) distribution for entire element and to determine relative burnup from element to element.

   a. Scan using Ge(Li) detector and multichannel analyzer for fission-product peaks in the energy range 100 to 1400 keV, including ^{106}Ru and ^{137}Cs.

   b. Scan longitudinally in 1.0-in. increments along centerline of element.

4. Measure Channel Gaps

   Purpose: To detect unusual amounts of plate swelling or warping.

   a. Remove end fittings.
   b. Measure channel gaps on both sides of comb.

1-4. Same as above.

5. Dismantling of Element

Purpose: To prepare plates for individual examination.

a. Separate individual fuel plates from side plates.

6. Visual Inspection of Plate

Purpose: To detect blisters or other unusual features.

a. Observe general external appearance of each plate and note any unusual features.

b. Photograph typical plates (2 or 3) and any areas of unusual features.

7. Thickness Measurements

Purpose: To provide data for estimation of plate swelling. Since measured thickness changes always overestimate the volume change (only the "high" points on the surface are measured), these measurements will serve mainly to show that no unexpected swelling has occurred.

a. Measure thickness at ~24 points on plates Nos. 1, 5, 9, 13, and 17, including at least two points outside the fuel meat zone.

b. Measure thickness at conspicuous spots.

8. Gamma Scanning

Purpose: To Determine relative longitudinal and transverse burnup (fission-product) distributions.

a. Perform analog scan longitudinally along centerline for all plates, for both integral above 0.5 MeV and ^{137}Cs.

b. Perform multichannel spectrum measurements along centerline at peak, as determined from analog scan, at 6 in. below peak, and at 10 in. above peak for plates Nos. 1, 5, 9, 13, and 17.

c. Perform analog scan transversely at peak of longitudinal scan, at 6 in. below peak, and at 10 in. above peak for plates Nos. 1 and 9, for both integral above 0.5 MeV and ^{137}Cs.

Table E-4. NSI-201 Coolant Channel Measurements

Channel	Bottom Side (mils)				Top Side (mils)			
	Max.	Min.	Avg.	At Peak Burnup	Max.	Min.	Avg.	At Peak Burnup
1	116.0	108.0	109.2	109.2	117.0	108.0	114.6	109.5
2	106.4	103.0	104.7	104.5	108.7	104.2	107.2	106.7
3	112.0	104.0	106.0	104.6	109.0	103.2	105.2	104.1
4	110.0	108.0	109.3	109.1	109.8	107.2	108.7	108.8
5	110.0	105.0	107.6	107.3	109.7	105.3	107.5	107.1
6	109.2	107.2	108.6	108.1	109.1	107.0	108.2	107.5
7	109.0	105.0	107.0	106.5	109.0	105.0	107.0	105.9
8	111.0	108.3	109.1	109.3	111.0	108.2	109.6	109.8
9	108.0	105.0	105.2	105.3	107.5	104.3	105.5	104.7
10	109.6	107.5	108.9	108.8	109.8	107.8	109.2	109.2
11	109.3	106.7	108.2	107.7	110.0	107.0	108.4	107.1
12	110.2	108.1	109.5	108.9	110.4	108.5	109.5	108.8
13	109.8	106.9	108.3	108.3	105.5	104.0	104.7	105.6
14	112.2	109.3	111.0	110.6	108.7	106.8	107.8	107.7
15	111.6	108.5	110.0	109.5	124.0	105.9	107.0	106.0
16	115.5	110.0	114.3	114.7	124.0	108.0	109.7	109.8
17	113.2	108.8	112.0	112.3	124.0	106.5	107.0	106.1
18	107.3	101.8	103.2	102.7	106.0	102.5	103.9	104.0
			Average	108.2			Average	107.1

APPENDIX F

PLATE THICKNESS MEASUREMENTS

This appendix presents the backup data for the plate thickness increases reported in Table VIII. The methods of measuring plate thickness are discussed in the text. In general, the plate thickness was measured at 26 locations on the plate. Along the length of the plate in eight locations, the thickness was measured in the center of the plate and near both edges. Two measurements were taken 1/4-inch from the top of the plates over the unfueled region. In calculating average thickness change for plate swelling, only the center measurements were used because of the additional uncertainties in the measurements near the edges due to the angle of the plate between the dial indicator tips. Since burnup is not uniform, thickness increases are compared at two locations--the maximum- and minimum-burnup locations. The minimum-burnup location is near the top of the plate and only the measurment at the 1-inch point was included. The peak-burnup region is larger and the 13- and 16-inch measurements were averaged. Although all plates of NSI-201 and NSI-202 were measured, only those plates in positions 2, 6, 10, 14, and 18 were included in the averages since only the plates in those positions were measured for the other four elements.

Table F.1
Element BSI-201
Plate Thickness and Incremental Thickness Compared to Ends (mils)

Distance From Top of Plate in.	Plate S-3-211-15 Position 2		Plate S-3-211-3 Position 6		Plate S-3-210-19 Position 10		Plate S-3-210-9 Position 14		Plate S-3-210-1 Position 18	
	t*	Δt	t*	Δt	t*	Δt	t*	Δt	t*	Δt
1/4	50.7	-	49.9	-	50.3	-	49.1**	-	49.9	-
1	50.7	0	49.9	0	50.3	0	49.8**	0.7	49.9	0
4	50.6	-0.1	49.7	-0.2	50.4	0.1	49.8	0.7	50.8	0.9
7	50.6	-0.1	49.8	-0.1	51.1	0.8	50.0	0.9	51.6	1.7
10	50.9	0.2	49.7	-0.2	51.8	1.5	50.5	1.4	52.7	2.8
13	50.6	-0.1	49.7	-0.2	52.0	1.7	51.0	1.9	53.2	3.3
16	50.9	0.2	50.3	0.4	52.1	1.8	51.0	1.9	53.7	3.8
19	50.7	0	49.6	-0.3	52.2	1.9	51.1	2.0	54.3	4.4
22	-	-	-	-	51.0	0.7	50.8	1.8	54.2	4.3

Average at 1 inch (low-burnup end) 0.1 mil

Average at 13 to 16 inches (peak-burnup region) 1.5 mils

*Plate thickness calculated by adding thickness change from plate end to preirradiation end tab thickness.

**Values determined by capacitance measuring device. Preirradiation end tab measured 50.3.

Table F.2
Element BSI-202
Plate Thickness and Incremental Thickness Compared to Ends (mils)

Distance From Top of Plate in.	Plate S-3-212-3 Position 2		Plate S-3-213-3 Position 6		Plate S-3-212-15 Position 10		Plate S-3-212-7 Position 14		Plate S-3-211-19 Position 18	
	t*	Δt	t*	Δt	t*	Δt	t*	Δt	t*	Δt
1/4	50.8	-	49.9**	-	50.1**	-	50.1	0	50.4	-
1	50.8	0	49.9**	0	50.1**	0	50.1	0	50.4	0
4	51.3	0.5	49.9	0	50.4	0.3	51.2	1.1	51.2	0.8
7	52.1	1.3	50.2	0.3	50.9	0.8	52.7	2.6	51.8	1.4
10	52.6	1.8	50.5	0.6	51.4	1.3	52.1	2.0	51.4	1.0
13	52.7	1.9	50.8	0.9	51.5	1.4	53.3	3.2	51.6	1.2
16	53.3	2.5	50.8**	0.9	51.5**	1.4	53.5	3.4	51.5	1.1
19	53.3	2.5	50.6	0.7	51.8	1.7	53.5	3.4	51.5	1.1
22	53.0	2.2	50.6	0.7	51.9	1.8	52.0	1.9	52.2	1.8

Average at 1 inch (low-burnup end) 0

Average at 13 to 16 inches (peak-burnup region) 1.8 mils

*Plate thickness calculated by adding thickness change from plate end to preirradiation end tab thickness.

**Plate thickness corroborated by new capacitance measuring device.

Table F.3
Element CSI-201
Plate Thickness and Incremental Thickness Compared to Ends (mils)

Distance From Top of Plate in.	Plate OSIEW-087 Position 1		Plate OSIIW-061 Position 5		Plate OSIIW-047 Position 9		Plate OSIIW-052 Position 13		Plate OSIIW-083 Position 17	
	t	Δt	t	Δt	t	Δt	t	Δt	t	Δt
1/4	*	-	*	-	*	-	*	-	*	-
1		0.5		1.2		-0.9		-0.6		0.5
4		1.3		0.6		0.5		1.0		0.5
7		1.6		0.6		0.5		1.2		1.4
10		2.3		0		1.1		2.1		1.0
13		2.8		0.7		1.3		2.7		0.9
16		2.8		0.4		1.5		3.0		1.3
19		2.7		1.7		2.2		2.6		0.9
22		2.9		0.6		1.4		2.2		1.4

Average at 1 inch (low-burnup end) 0.1 mil

Average at 13 to 16 inches (peak-burnup region) 1.7 mils

*Actual plate thicknesses are not calculated due to erroneous standard readings. Thickness changes are measured relative to the plate thickness at 1/4" over the unfueled region.

Table F.4
Element CSI-202
Plate Thickness and Incremental Thickness Compared to Ends (mils)

Distance From Top of Plate in.	Plate OSIIW-085 Position 2		Plate OSIIW-079 Position 6		Plate OSIIW-063 Position 10		Plate OSIIW-039 Position 14		Plate OSIIW-075 Position 18	
	t*	Δt	t*	Δt	t*	Δt	t*	Δt	t*	Δt
1/4	50.0	-	50.0	-	50.4	-	49.2	-	49.4	-
1	51.0	1.0	50.5	0.5	50.9	0.5	49.7	0.5	49.6	0.2
4	51.4	1.4	52.6	2.6	52.6	2.2	50.5	1.3	51.6	2.2
7	52.9	2.9	52.6	2.6	53.1	2.7	51.7	2.5	53.3	3.9
10	53.6	3.6	53.9	3.9	53.5	3.1	52.2	3.0	54.4	5.0
13	55.8	5.8	55.2	5.2	53.6	3.2	53.3	4.1	54.9	5.5
16	52.8	2.8	55.2	5.2	53.8	3.4	53.0	3.8	54.1	4.7
19	52.2	2.2	54.4	4.4	53.6	3.2	52.4	3.2	53.7	4.3
22	50.5	0.5	53.3	3.3	54.6	4.2	50.9	1.7	53.6	4.2

Average at 1 inch (low-burnup end) 0.5 mil

Average at 13 to 16 inches (peak-burnup region) 4.4 mils

*Plate thickness calculated by adding thickness change from plate end to preirradiation end tab thickness.

Table F.5
Element NSI-201
Plate Thickness and Incremental Thickness Compared to Ends (mils)

Distance From Top of Plate in.	Plate ORR-92 Position 2		Plate ORR-97 Position 6		Plate ORR-102 Position 10		Plate ORR-106 Position 14		Plate ORR-110 Position 18	
	t*	Δt	t*	Δt	t*	Δt	t*	Δt	t*	Δt
1/4	49.2	-	48.7	-	49.0	-	49.0	-	49.2	-
1	48.8	-0.4	49.8	1.1	50.1	1.1	49.8	0.8	50.2	1.0
4	48.9	-0.3	50.0	1.3	50.1	1.1	50.1	1.1	50.0	0.8
7	48.7	-0.5	50.0	1.3	50.0	1.0	50.0	1.0	50.2	1.0
10	48.8	-0.4	50.1	1.4	50.0	1.0	50.3	1.3	50.3	1.1
13	49.4	0.2	50.2	1.5	50.1	1.1	50.2	1.2	50.2	1.0
16	49.2	0	50.0	1.3	50.1	1.1	50.0	1.0	50.3	1.1
19	49.2	0	49.9	1.2	50.1	1.1	50.3	1.3	50.4	1.2
22	49.7	0.5	50.1	1.4	50.0	1.0	50.3	1.3	50.5	1.3

Δt average at 1 inch (low-burnup end) 0.7 mil

Δt average at 13 to 16 inches (peak-burnup region) 1.0 mils

*Plate thickness based on comparison to standard with thickness change calculated from plate end tabs postirradiation measurement.

Table F.6
Element NSI-202
Plate Thickness and Incremental Thickness Compared to Ends (mils)

Distance From Top of Plate in.	Plate ORR-120 Position 7		Plate ORR-121 Position 8		Plate ORR-131 Position 15		Plate ORR-139 Position 17		Plate ORR-140 Position 18	
	t*	Δt	t*	Δt	t*	Δt	t*	Δt	t*	Δt
1/4	50.6	-	50.0	-	51.1	-	50.7	-	51.2	-
1	51.8	1.2	51.6	1.6	51.7	0.6	52.0	1.3	51.7	0.5
4	52.8	2.2	53.4	3.4	52.4	1.3	52.4	1.7	53.2	2.0
7	53.0	2.4	57.8	2.8	53.0	1.9	52.9	2.2	54.4	3.2
10	53.6	3.0	53.4	3.4	54.0	2.9	53.5	2.8	55.5	4.1
13	54.3	3.7	54.2	4.2	54.5	3.4	53.9	3.2	56.2	5.0
16	55.0	4.4	54.7	4.7	54.5	3.4	54.6	3.9	56.7	5.5
19	55.1	4.5	54.5	4.5	55.0	3.9	54.5	3.8	56.6	5.4
22	55.6	5.0	54.1	4.1	54.2	3.1	54.0	3.3	56.8	5.6

Average at 1 inch (low-burnup end) 1.0 mil

Average at 13 to 16 inches (peak-burnup region) 4.1 mils

*Plate thickness based on comparison to standard with thickness change calculated from plate end tabs postirradiation measurement.

APPENDIX G

PLATE GAMMA SCANNING DATA AND BURNUP ANALYSIS

Correlation of Gamma Scanning and Burnup Data - As discussed in the text, several methods of taking and recording gamma scanning data were used over the course of this work. The gamma scan profile was used to select the axial minimum- and maximum-burnup locations for the burnup analysis samples. Full width sections were removed from one plate of each element at these locations and analyzed by mass spectrometry to determine the burnup (see below). To obtain the average burnup at the low- and maximum-burnup positions, the ^{137}Cs peak as measured by the NaI crystal and strip chart was used. The chart readings at the minimum were averaged and the ratio of the average to the reading of the analyzed plate was multiplied by the analyzed burnup value. The same method was used for finding the average burnup at the axial maximum. To find the average burnup along the length of the plates (and hence elements), the chart readings were averaged along the length of the charts at one-inch intervals (about 35 readings per chart). This gives a bias toward a low average since the minimum-to-maximum ratios of the readings are consistently lower than those of the analyzed burnups. Such a discrepancy could result if a plate had different transverse burnup profiles at the minimum- and maximum-burnup positions since only the central part of the plate was scanned while the entire width of the plate was averaged in the burnup analyses. The same five plates were used for the minimum- and maximum-burnup location averages as were used for the thickness measurements.

The data obtained using the Ge(Li) detector and the multichannel analyzer are believed to be more accurate than the analog data obtained using the NaI crystal for determining the burnup profile through an element. Therefore, these data were used for elements BSI-201, BSI-202, CSI-201, and NSI-202. As explained in Table G.4, the multichannel data appeared to be discrepant for the plate in position 18 of CSI-202. Multichannel data were not obtained for all plates of NSI-201. The analog data were used for these two elements. The element was assumed to have the axial profile of the plate from which the burnup analysis sample was taken, and the analyzed maximum burnup was used. The data and correlation calculations are presented in Tables G.1 through G.6. Examples of the analog gamma scan charts are shown in Figs. G.1 through G.6.

Burnup Calculation from Isotopic Analysis - The isotopic composition of the uranium and plutonium after irradiation can be used to calculate the burnup or percentage depletion of the original ^{235}U in the elements. The isotopic abundance data as determined by mass spectrographic analysis are presented in Table G.7.

The burnup can be expressed in terms of the pre- and postirradiation ^{235}U isotopic abundances, as shown in the following. Let

B = fractional ^{235}U depletion (burnup),
A_o = fractional ^{235}U atomic abundance prior to irradiation,
A = fractional ^{235}U atomic abundance after irradiation,
C = $^{238}U/^{235}U$ atomic depletion ratio during irradiation,
and D = $^{236}U/^{235}U$ atomic depletion ratio during irradiation (negative quantity).

Now,
$$B = 1 - \frac{AN}{A_o N_o} ,$$

where N_o and N represent the pre- and postirradiation uranium atom densities. If ΔN^5 represents the change in ^{235}U atom density during irradiation,

$$N = N_o - (1 + C + D)\Delta N^5$$

and
$$B = 1 - \frac{AN_o - (1 + C + D)A\Delta N^5}{A_o N_o}$$

$$= 1 - A/A_o + (1 + C + D)AB.$$

Therefore,
$$B = \frac{1 - A/A_o}{1 - (1 + C + D)A} \qquad (1)$$

The parameters C and D have been derived from the results of integral transport cell calculations performed at ANL by M. M. Bretscher and R. J. Cornella. They behave as follows:

	LEU		MEU	
B	C	D	C	D
0.54	0.13	-0.16	0.06	-0.16
0.76	0.15	-0.15	0.07	-0.16
0.89	0.18	-0.15	0.08	-0.15
0.96	0.22	-0.14	0.10	-0.15
0.98	0.26	-0.14	0.10	-0.14

It appears that C and D are not particularly sensitive to the uranium density. There is obviously a dependence of C on the enrichment; however, there is a very weak dependence of B on either C or D, as indicated by Eq. 2, since A is small (<0.20 for LEU).

$$\frac{\partial B}{\partial C} = \frac{\partial B}{\partial D} = \frac{AB}{1 - (1 + C + D)A} \qquad (2)$$

Therefore, the calculations from which C and D are derived do not have to be extremely accurate.

As used in Eq. 1, A and A_o are atomic ratios while the enrichment, e, is a weight ratio. The relationship between A_o and e_o is

$$A_o = \frac{1}{1 + 0.98736(1/e_o - 1)} \qquad (3)$$

The fission density due to ^{235}U fission alone (F_{DU}) can be derived as follows:

$$B = \frac{N_F + N_C}{N}$$

where N_F, N_C, and N are the densities of ^{235}U fissions, ^{235}U captures, and originally contained ^{235}U atoms, respectively.

$$N_F + N_C = N_F(1 + \alpha)$$

where α = the ^{235}U capture-to-fission ratio.

$$N = \frac{6.022 \times 10^{21}\ \rho_U e}{235.04}$$

Therefore, substituting the symbol F_{DU} for N_F,

$$F_{DU} = \frac{2.562 \times 10^{21}\ \rho_U eB}{1 + \alpha}$$

Assuming an average value of 0.19 for α over the burnup of the fuel,

$$F_{DU} = 2.15 \times 10^{21}\ \rho_U eB \qquad \text{(fissions/cm}^3\text{)}. \qquad (4)$$

Integral transport cell depletion calculations, performed at ANL by R. J. Cornella, provided the ^{235}U fission fraction as a function of ^{235}U depletion. The cumulative fission fraction is plotted as a function of ^{235}U burnup in Fig. G.8 for 20%-enriched (LEU) and 45%-enriched (MEU) fuel. The result of Eq. (4), divided by the appropriate fission fraction, gives the absolute fission density. Burnups, fission fractions, and fission densities of the analyzed samples are given in Table G.8.

It was the intent early in the RERTR Program to determine absolute fission densities based upon ^{148}Nd measurements. The results of such determinations were found to be unreliable, for undetermined reasons. Therefore, acquisition and use of ^{148}Nd data were abandoned.

Table G.1.
Element BSI-201
Burnup Analysis Plate S-3-210-1, Position 18

Calculation of Plate Average

	^{137}Cs, 10^3 Cts/s	Burnup % ^{235}U Depletion
Minimum	22.5	$\frac{22.5}{24.0} \times 31.5 = 29.5$
At Top Analysis Point	24.0	31.5
Maximum (Bottom Analysis Point)	62.5	70.9
Average	48.4	$\frac{48.4}{62.5} \times 70.9 = 54.9$

Calculation of Element Average

Plate Position	^{137}Cs, 10^3 Cts/s		
	Minimum	Maximum	Average
2	21.0	62.5	48.3
6	21.0	57.0	44.9
10	20.5	60.0	45.5
14	21.5	61.5	47.3
18	22.5	62.5	48.4
Average	21.3	60.7	46.9
Correlated Average Burnup	$\frac{21.3}{22.5} \times 29.5 =$ 28.0	$\frac{60.7}{62.5} \times 70.9 =$ 68.9	$\frac{46.9}{48.4} \times 54.9 =$ 53.2

^{137}Cs peak measured by multichannel analyzer gave the following counts/s at the maximum-burnup position for plates 1 through 19: 141.8, 156.1, 157.9, 150.0, 148.9, 146.3, 154.5, 152.1, 146.9, 149.0, 154.2, 150.9, 155.0, 150.7, 154.6, 152.5, 162.9, 154.3, and 151.9. The average of 152.1 correlates to an element average burnup of 54.1% using all 19 plates.

Table G.2.

Element NSI-202

Burnup Analysis Plate S-3-211-19, Position 18

Calculation of Plate Average

	^{137}Cs, 10^3 Cts/s	Burnup % ^{235}U Depletion
Minimum	115	$\frac{115}{115} \times 50.5 = 50.5$
At Top Analysis Point	115	50.5
Maximum (Bottom Analysis Point)	315	97.3
Average	259	$\frac{259}{315} \times 97.3 = 80.0$

Calculation of Element Average

Plate Position	^{137}Cs, 10^3 Cts/s Minimum	Maximum	Average
2	115	320	269
6	130	310	265
10	125	310	262
14	120	310	260
18	115	315	259
Average	121	313	263
Correlated Average Burnup	$\frac{121}{115} \times 50.5 =$ 53.1	$\frac{313}{315} \times 97.3 =$ 96.7	$\frac{263}{259} \times 80.0$ 81.2

^{137}Cs peak measured by multichannel analyzer gave the following counts/s at the maximum-burnup position for plates 1 through 19: 239.2, 250.2, 237.5, 264.2, 252.5, 239.5, 231.4, 253.0, 226.1, 235.4, 248.8, 240.1, 233.3, 245.9, 228.4, 233.3, 243.8, 250.3, and 252.1. The average of 242.4 correlates to an element average burnup of 77.5% using all 19 plates.

Table G.3.

Element CSI-201

Burnup Analysis Plate OSIIW-084, Position 18

Calculation of Plate Average

	^{137}Cs, 10^3 Cts/s	Burnup % ^{235}U Depletion
Minimum	17.0	$\frac{17.0}{17.5} \times 32.7 = 31.8$
At Top Analysis Point	17.5	32.7
Maximum (Bottom Analysis Point)	45.5	66.9
Average	36.7	$\frac{36.7}{45.5} \times 66.8 = 54.0$

Calculation of Element Average

Plate Position	^{137}Cs, 10^3 Cts/s		
	Minimum	Maximum	Average
2	17.0	46.0	38.0
6	17.0	43.5	34.7
10	16.5	45.0	36.0
14	17.0	44.0	34.6
18	17.0	45.5	36.7
Average	16.9	44.8	36.0
Correlated Average Burnup	$\frac{16.9}{17.0} \times 31.8 =$ 31.6	$\frac{44.8}{45.5} \times 66.8 =$ 65.8	$\frac{36.0}{36.7} \times 54.0 =$ 53.0

^{137}Cs peak measured by multichannel analyzer gave the following counts/s at the maximum-burnup position for plates 1 through 19: 714.2, 575.8, 662.1, 646.8, 568.6, 541.5, 545.9, 610.9, 584.9, 608.4, 602.0, 615.6, 594.2, 600.7, 604.2, 607.2, 611.1, 627.4, and 656.5. The average of 609.4 correlates to an element average burnup of 52.4% using all 19 plates.

Table G.4.

Element CSI-202

Burnup Analysis Plate OSIIW-075, Position 18

Calculation of Plate Average

	^{137}Cs, 10^3 Cts/s	Burnup % ^{235}U Depletion
Minimum	105	$\frac{105}{105} \times 55.0 = 55.0$
At Top Analysis Point	105	55.0
Maximum (Bottom Analysis Point)	290	96.6
Average	245	$\frac{245}{290} \times 96.6 = 81.6$

Calculation of Element Average

Plate Position	^{137}Cs, 10^3 Cts/s		
	Minimum	Maximum	Average
2	115	300	251
6	130	300	246
10	135	290	240
14	130	295	241
18	105	290	245
Average	123	295	245
Correlated Average Burnup	$\frac{123}{105} \times 55.0 =$ 64.4	$\frac{295}{290} \times 96.6 =$ 98.3	$\frac{245}{245} \times 81.7 =$ 81.7

^{137}Cs peak measured by multichannel analyzer gave the following counts/s at the maximum-burnup position for plates 1 through 19: 259.6, 232.6, 239.8, 235.8, 251.7, 248.4, 249.0, 235.6, 257.5, 240.1, 242.9, 236.0, 237.4, 234.9, 235.8, 232.2, 237.7, 228.8, and 239.9. The average of 240.8 was not used to correlate to an average element burnup because the value for plate 18 is obviously low and results in unphysically high burnups for many of the plates.

Table G.5.
Element NSI-201
Burnup Analysis Plate ORR-93, Position 3

Calculation of Plate Average

	^{137}Cs, 10^3 Cts/s	Burnup % ^{235}U Depletion
Minimum	21.5	$\frac{21.5}{23.0} \times 24.1 = 22.5$
At Top Analysis Point	23.0	24.1
Maximum (Bottom Analysis Point)	55.0	50.9
Average	43.0	$\frac{43}{55} \times 50.9 = 39.8$

Calculation of Element Average

Plate Position	^{137}Cs, 10^3 Cts/s Minimum	Maximum	Average
1	21.0	51.0	40.1
2	20.0	53.5	41.5
3	21.5	55.0	43.0
4	19.0	52.0	39.6
5	18.5	50.5	38.5
6	17.0	47.0	35.9
7	16.5	47.0	35.7
8	21.5	54.0	42.0
9	16.5	46.0	34.6
10	19.0	52.0	39.6
11	15.5	45.0	33.8
12	16.0	45.5	34.5
13	17.0	48.5	37.2
14	16.0	46.0	34.8
15	17.0	48.5	36.5
16	16.5	46.5	35.5
17	16.5	47.0	35.7
18	16.5	47.5	35.8
19	21.0	54.5	41.9
Average	18.0	49.3	37.7
(Plates 2, 6, 10, 14, 18)	17.7	49.2	37.5
Correlated Average Burnup	$\frac{18.0}{21.5} \times 22.5 =$	$\frac{49.3}{55.0} \times 50.9 =$	$\frac{37.7}{43.0} \times 39.8 =$
(19 Plates)	18.9	45.6	34.9
(Plates 2, 6, 10, 14, 18)	18.5	45.5	34.7

Table G.6.

Element NSI-202

Burnup Analysis Plate ORR-140, Position 18

Calculation of Plate Average

	^{137}Cs, 10^3 Cts/s	Burnup % ^{235}U Depletion
Minimum	22.0	$\frac{22.0}{22.5} \times 54.2 = 53.0$
At Top Analysis Point	22.5	54.2
Maximum (Bottom Analysis Point)	49.0	96.4
Average	43.4	$\frac{43.4}{49.0} \times 96.4 = 85.4$

Calculation of Element Average

Plate Position	^{137}Cs, 10^3 Cts/s		
	Minimum	Maximum	Average
2	20.0	48.5	41.9
6	22.0	50.0	43.3
10	22.5	50.0	44.1
14	22.5	50.0	43.7
18	22.0	49.0	43.4
Average	21.8	49.5	43.3
Correlated Average Burnup	$\frac{21.8}{22.0} \times 53.0 =$ 52.5	$\frac{49.5}{49.0} \times 96.4 =$ 97.4	$\frac{43.3}{43.4} \times 85.5 =$ 85.3

^{137}Cs peak measured by multichannel analyzer gave the following counts/s at the maximum-burnup position for plates 1 through 19: 102.5, 97.4, 100.4, 98.0, 98.5, 100.0, 93.5,, 95.6, 97.8, 97.0, 95.4, 94.5, 92.9, 92.8, 95.4, 96.5,. 99.3, 100.9, and 100.0. The average of 97.3 correlates to an element average burnup of 82.4% using all 19 plates.

Table G.7. Final Isotopic Composition of Uranium and Plutonium

Element Number	BSI-201		BSI-202	
Plate Number	S-3-210-1		S-3-211-19	
	Top	Bottom	Top	Bottom
^{234}U	0.111	0.097	0.104	0.068
^{235}U	14.62	6.81	11.01	0.700
^{236}U	1.254	2.73	1.962	3.737
^{238}U	84.01	90.37	86.92	95.495
^{238}Pu	0.240	1.46	0.833	5.86
^{239}Pu	86.91	66.41	77.28	45.53
^{240}Pu	10.18	20.09	14.42	22.74
^{241}Pu	2.48	9.05	6.49	10.70
^{242}Pu	0.187	3.00	0.973	15.16

Element Number	CSI-201		CSI-202	
Plate Number	OSIIW-084		OSIIW-075	
	Top	Bottom	Top	Bottom
^{234}U	0.110	0.100	0.107	0.068
^{235}U	14.400	7.644	10.11	0.852
^{235}U	1.253	2.537	2.092	3.67
^{238}U	84.237	89.718	87.69	95.41
^{238}Pu	0.236	1.271	0.889	5.41
^{239}Pu	86.566	68.216	75.81	47.19
^{240}Pu	10.472	19.638	15.53	22.72
^{241}Pu	2.530	8.427	6.63	10.71
^{242}Pu	0.196	2.449	1.135	13.97

Element Number	NSI-201		NSI-202		NSI-202
Plate Number	ORR-093		ORR-140		ORR-145
	Top	Bottom	Top	Bottom	Outside Plate, #1 Near Peak
^{234}U	0.111	0.104	0.107	0.068	0.078
^{235}U	15.820	10.530	10.168	0.893	1.238
^{235}U	0.932	1.935	2.031	3.620	3.580
^{238}U	83.138	87.131	87.694	95.413	95.104
^{238}Pu	0.134	0.701	0.894	5.423	4.792
^{239}Pu	90.276	76.650	75.368	47.211	49.442
^{240}Pu	8.086	15.362	15.841	22.574	20.773
^{241}Pu	1.432	6.308	6.758	11.191	12.567
^{242}Pu	0.071	0.960	1.126	13.601	12.424

COMMITTEE TO BRIDGE THE GAP
1637 BUTLER AVENUE #203
LOS ANGELES, CALIFORNIA 90025
(213) 478-0829

December 10, 1987

Director
Division of Rules and Records
Office of Administration
U.S. Nuclear Regulatory Commission
Washington, D.C. 20555

FREEDOM OF INFORMATION ACT REQUEST
FOIA-87-825
Rec'd 12-14-87

Ref: FOIA 87-180

Dear Sir or Madam:

This is a request under the Freedom of Information Act.

In 1986 the Commission adopted a new rule (10 C.F.R. §50.64) that generally requires licensees that use highly enriched uranium fuel to convert their facilities to low enriched uranium.

We request a copy of the following documents pertaining to the new rule which have become available since our similar request of March 1987 (FOIA 87-180):

(1) All schedules for conversion which have been submitted to date in response to the new rule, together with supporting documentation.

(2) All requests for a unique purpose exemption, together with supporting documentation; or withdrawal of such requests.

(3) All other correspondence between NRC and licensees pertaining to the new rule.

(4) All correspondence between NRC and DOE or other federal agencies pertaining to the new rule or its implementation.

(5) Documents that address the conversion of industry reactors and the funding of such conversion.

We request that these documents be placed in the Public Document Room. We would appreciate it if, in addition, subject documents that are already in the PDR could be identified.

Thank you.

Sincerely,

Steven Aftergood
Executive Director

8802110068 1p.

INEL
Idaho National Engineering Laboratory

May 18, 1987

Mr. Mayo Carrington, Project Manager
U.S. Nuclear Regulatory Commission
Office of Nuclear reactor regulation
Technical Assistance Management Branch
Planning and Program analysis Staff
7920 Norfolk Avenue
Bethesda, MD 20014

SPERT FUEL REQUALIFICATION TECHNICAL EVALUATION REPORT - Oben-71-87

Dear Mr. Carrington:

Enclosed is the Technical Evaluation Report for the SPERT Fuel Review for use in Non-Power Reactors. This report has received INEL management review and is submitted as part of Task 3, NPR Reviews Associated With Conversion of Cores from HEU to LEU, of the NRC Form 189 for FIN D6010.

Please contact C. H. Cooper (FTS) 583-9183 regarding any additional matters with this enclosure:

Very truly yours,

CFObenchain

C. F. Obenchain, Manager
NRR and I&E Support

CHC:ggo

Enclosure:
As Stated

cc: H. Berkow, NRC
R. Carter, NRC ← pls return
T. Michaels, NRC
G. L. Jones, DOE-ID
J. O. Zane, EG&G Idaho (w/o Enclosure)

EG&G Idaho, Inc. P.O. Box 1625 Idaho Falls, ID 83415

D11

EGG-NTA-7708

TECHNICAL EVALUATION REPORT FOR THE REQUALIFICATION OF SPERT FUEL FOR USE IN NON-POWER REACTORS

R. R. Hobbins

Published May 1987

EG&G Idaho, Inc.
Idaho Falls, Idaho 83415

Prepared for the
U.S. Nuclear Regulatory Commission
Washington, D.C. 20555
Under DOE Contract No. DE-AC07-76ID01570
FIN No. D6010

ABSTRACT

This report evaluates the requalification of SPERT fuel pins for use in non-power reactors. The requalification of SPERT fuel was performed by Argonne National Laboratory to verify that the pins have suffered no physical damage since fabrication. Pins were inspected under 6X magnification, and by x-radiographic, destructive, and metallographic examinations. Spectrographic and chemical analyses were performed on the UO_2 fuel. The requalification results give reasonable assurance that the SPERT fuel rods are suitable for use in non-power reactors provided that the effects of thin-wall defects in the region of the upper end cap and low-density fuel pellets are evaluated for the intended operating conditions.

FIN No. D6010--Casework and Non-Power Reactor Reviews

CONTENTS

TECHNICAL EVALUATION REPORT FOR THE REQUALIFICATION OF SPERT FUEL FOR USE IN NON-POWER REACTORS

INTRODUCTION

Some universities are considering converting their non-power reactors to low enrichment fuel by use of stainless steel clad, UO_2 fuel pins manufactured in the 1960s for use in the Special Power Excursion Reactor Test (SPERT) program. The 600 SPERT fuel pins, whose serial numbers cover virtually the entire range of serial numbers of the 9000 pins produced, were examined in the requalification program conducted by Argonne National Laboratory (ANL).[1] The 600 pins examined by ANL had never been used in a reactor and had been in air-conditioned storage at Purdue University since 1974. There is no record of the storage conditions between 1965 and 1974. The results of the ANL requalification program should be applicable to the entire production run of SPERT pins, except for pins that have been operated in reactors or stored in water or under other conditions significantly different than the storage at Purdue. In these cases, examinations for corrosion of the cladding, both surface and intergranular, may be needed. Additional examination requirements for pins that have been used in reactors may need to be addressed on a case-by-case basis, depending on operational history.

REQUALIFICATION OF SPERT FUEL

The SPERT fuel pins originally were procured according to Phillips Specification No. F-1-SPT, which incorporates Phillips Drawing No. SPT-E-1166. The component materials were required to meet applicable ASTM standards; extensive acceptance tests and inspections were required for components and the finished pins. In particular, all pins were to be inspected for dimensions and surface condition, helium leak tested to ensure the integrity of the welds (the pins were filled with helium at the time of welding), and gamma scanned to check the fuel zone length and detect the presence of any foreign materials in the fuel zone. However, it appears that all fabrication, inspection, and acceptance records have been discarded. The purposes of the requalification program were to verify that the pins are those procured to Specification No. F-1-SPT, and that the pins have suffered no physical damage since fabrication.

All 600 pins were checked for straightness and examined under 6X magnification for nicks, scratches, and/or other damage to the cladding surface. Thirty rods were measured to check diameter and roundness. All pins appeared to be in excellent condition and met the dimensional and surface condition requirements of the specifications, except (possibly) for the diameter in the end cap welds that, on the average, is 0.0041 in. (0.10 mm) larger than the maximum dimension for the pin diameter given on the specification drawing.

Sixty pins were selected randomly among the representative groups of serial numbers for x-radiographic examination of the upper and lower end cap welds. Defects were found in the upper end cap welds on six pins. The x-radiography examination found the minimum wall thickness in the defects to vary from 0.005 to 0.015 in. (0.13 to 0.38 mm) [nominal cladding wall thickness is 0.020 in. (0.51 mm)]. Metallographic examination of one of the weld defects revealed it probably was caused by a gas bubble. Although this particular defect was not connected to the interior volume of the fuel pin, radiographs of other pins showing similar defects indicate that some of the defects are probably connected to the interior volume. These defects would not have been discovered at the time of fabrication because x-radiography was not specified.

Thin wall defects tend to produce stress concentrations at the defects. The effects of such stress concentrations should be evaluated for the intended use of the fuel pins. Factors such as differential pressure across the wall of the fuel pin during normal operation and under postulated accident conditions, fuel handling practices, and corrosion control should be considered. For some uses, 100% x-radiographic inspection to eliminate pins with thin wall defects may be advisable.

The internal pressure, void volume, and fill-gas composition were measured in five pins chosen for destructive examination, in addition to the pin whose weld defect was examined metallographically. All six pins had a positive pressure of fill-gas, ranging from 0.6 to 3.3 psig. For comparison, the specification for fill gas was 1 psig of helium. The fill gas was predominantly helium, but a sizable amount of hydrogen was also found (up to 16%). Trace amounts of water vapor and nitrogen were measured, although in one pin about 1% nitrogen and a few milligrams of water were found. The hydrogen is responsible for the overpressure in the pins. The hydrogen probably resulted from the reaction of water vapor with the fuel and the cladding. Less than 2 mg of water is required to produce the amounts of hydrogen measured in the fill gas. The specification allowed up to 75 ppm water in a fuel pin, which corresponds to about 60 mg. The presence of hydrogen in the fill gas has no deleterious effect because its thermal conductivity is nearly the same as that of helium. The other minor deviations in composition and pressure relative to the specifications have no significance for the use of these pins in non-power reactors.

The entire stack of 60 fuel pellets was examined from 2 pins, and the top 6 pellets were examined from 2 other pins. All pellets examined, with three exceptions, had only minor surface chips and were judged to meet the pellet surface condition requirements of specification F-1-SPT. Three pellets in one pin each had a significant piece (0.2, 0.2, and 0.7 g, respectively) spalled off the entire length of the pellet. The missing material was contained in loose fragments and powder collected after all the pellets were removed from the pin. The length, diameter, and weight of each of the 132 pellets removed from the four pins were measured and the

pellet density calculated based on solid, right, cylindrical geometry. Neglecting the three chipped pellets, sixteen pellets were found with densities outside the specification of 9.97 g/cm^3 minimum density and ±0.1 g/cm^3 deviation from the mean. Four pellets at the top of one pin were found with a density of about 9.52 g/cm^3. Excluding these four pellets and the three chipped pellets, the mean pellet density was 10.078 ± 0.055 g/cm^3. Twelve pellets in one rod had densities more than 0.1 g/cm^3 above the mean density, the largest of which was 0.15 g/cm^3 higher than the mean. With the exception of the four pellets with a relatively low density (9.52 g/cm^3), deviations of this magnitude from the specification for pellet density have no safety significance for the use of the SPERT fuel in non-power reactors. It is assumed that the pin with the four low-density pellets at the top of the fuel stack was purposely loaded in this manner and that the use of pellets with nonconforming densities was properly approved. Depending on the reactor power levels, low-density fuel pellets tend to run at higher temperatures, are subject to densification, enhanced fission-product release, and can promote exaggerated cladding collapse and pellet-cladding mechanical inter[illegible] The presence of low-density fuel pellets in other fuel pins an[illegible] stack locations cannot be ruled out with the current limited dat[illegible]e on fuel pellet density. The effects of low-density pellets should be evaluated for the intended use. Additional pellet density measurements to ensure that low-density pellets are an unlikely occurrence may be needed.

Three pellets, one from each of three rods, were sectioned and examined metallographically. The microstructures were similar in the three pellets and were relatively fine grained (5 to 10 μm) UO_2 with some porosity and, possibly, some U_4O_7 present. The structures are fairly typical of as-fabricated, unirradiated UO_2 fuel.

Analyses of uranium isotopes, total uranium, and impurities in the UO_2 fuel were performed. Spectrographic analysis for 20 elements revealed an impurity content of <185 ppm, which is only about 5% of the allowable level; however, a number of possible significant elements were

not analyzed. An upper limit value of the oxygen/uranium ratio of 2.04 was calculated, based on the measured uranium content, measured impurity content, and the assumption that the remaining sample weight must be oxygen. An additional impurity content of 1200 ppm, which would be well within the specification, would result in an oxygen/uranium ratio of 2.02, which is the specified upper bound.

Metallographic examination of the fuel rod cladding showed the cladding to be within specification for wall thickness; to be seamless, as specified; and to have a microstructure typical of 304 stainless steel with some evidence of normal carbide precipitation, but no evidence of intergranular attack or corrosion from either the inside or outside surfaces. Chemical analysis showed that the metallic constituents of the stainless steel were all within the specification with the exception of cobalt, which was 0.084 wt% compared to a maximum allowable of 0.05 wt%.

CONCLUSIONS

It is concluded that the ANL examinations give reasonable assurance that these SPERT fuel pins were fabricated in accordance with Phillips Specification No. F-1-SPT, and that they substantially met the acceptance criteria when fabricated. Furthermore, the examinations show that storage for more than 20 years has not caused deterioration to cladding or pellets that would significantly affect safety in the use of these fuel pins in low power reactors. Therefore, these fuel pins are acceptable for use if the operating conditions do not cause undue stresses in the cladding. At high reactor power levels, there might be some concern because of the presence of thin-wall defects and low-density fuel pellets, but these factors should be evaluated for the intended fuel use on a case-by-case basis. The deviations from such specifications as pin internal pressure and fuel oxygen/uranium ratio are minor and without significance from a safety standpoint. The absence of intergranular attack or corrosion of the stainless-steel cladding during storage, and the basic conformance of the stainless-steel cladding to the specifications, suggest that corrosion is an unlikely failure mechanism provided there is reasonable water chemistry control.

REFERENCES

1. J. L. Snelgrove, R. F. Domagala, L. R. Dates, Requalification of SPERT Fuel Pins for Use in University Reactors, ANL/RERTR-TM-8, December 1986.

NRC FORM 335 (2-84) NRCM 1102, 3201, 3202

U.S. NUCLEAR REGULATORY COMMISSION

BIBLIOGRAPHIC DATA SHEET

SEE INSTRUCTIONS ON THE REVERSE

1 REPORT NUMBER (Assigned by TIDC, add Vol. No., if any)

EGG-NTA-7708

2 TITLE AND SUBTITLE

TECHNICAL EVALUATION REPORT FOR THE REQUALIFICATION OF SPERT FUEL FOR USE IN NON-POWER REACTORS

3 LEAVE BLANK

4 DATE REPORT COMPLETED

MONTH	YEAR
May	1987

5 AUTHOR(S)

R. R. Hobbins

6 DATE REPORT ISSUED

MONTH	YEAR
May	1987

7 PERFORMING ORGANIZATION NAME AND MAILING ADDRESS (Include Zip Code)

NRR and I&E Support
EG&G Idaho, Inc.
P. O. Box 1625
Idaho Falls, ID 83415

8 PROJECT/TASK/WORK UNIT NUMBER

9 FIN OR GRANT NUMBER

D6010

10 SPONSORING ORGANIZATION NAME AND MAILING ADDRESS (Include Zip Code)

11a TYPE OF REPORT

b PERIOD COVERED (Inclusive dates)

12 SUPPLEMENTARY NOTES

13 ABSTRACT (200 words or less)

This report evaluates the requalification of SPERT fuel pins for use in non-power reactors. The requalification of SPERT fuel was performed by Argonne National Laboratory to verify that the pins have suffered no physical damage since fabrication. Pins were inspected under 6X magnification, and by x-radiographic, destructive, and metallographic examinations. Spectrographic and chemical analyses were performed on the UO_2 fuel. The requalification results give reasonable assurance that the SPERT fuel rods are suitable for use in non-power reactors provided that the effects of thin-wall defects in the region of the upper end cap and low-density fuel pellets are evaluated for the intended operating conditions.

14 DOCUMENT ANALYSIS - a KEYWORDS/DESCRIPTORS

b IDENTIFIERS/OPEN-ENDED TERMS

15 AVAILABILITY STATEMENT

Unlimited

16 SECURITY CLASSIFICATION

(This page)
Unclassified

(This report)
Unclassified

17 NUMBER OF PAGES

18 PRICE